The impact of aging on spreading depolarization in the intact and ischemic rat brain

PhD Thesis

Menyhárt Ákos

Szeged, 2017

University of Szeged
Faculty of Medicine, Faculty of Science and Informatics
Department of Medical Physics and Informatics

The impact of aging on spreading depolarization in the intact and ischemic rat brain

PhD Thesis

Menyhárt Ákos

Supervisor: Dr. Farkas Eszter
Doctoral School of Theoretical Medicine

Szeged, 2017

Publications related to the PhD thesis

I. Menyhárt Á., Makra P, Szepes BT, Tóth OM, Hertelendy P, Bari F, Farkas E

High incidence of adverse cerebral blood flow responses to spreading depolarization in the aged ischemic rat brain

***NEUROBIOLOGY OF AGING* 36:**(12) pp. 3269-3277. (2015)

Folyóirat szakterülete: Geriatrics and Gerontology helyzete: 3/108 (D1)

II. Ákos Menyhárt, Dániel Zölei-Szénási, Tamás Puskás, Péter Makra, Orsolya M.Tóth, Borbála É. Szepes, Réka Tóth, Orsolya Iványkovits-Kiss, Tihomir P. Obrenovitch, Ferenc Bari, Eszter Farkas

Spreading depolarization remarkably exacerbates ischemia-induced tissue acidosis in the young and aged rat brain

SCIENTIFIC REPORTS: 2017, in press

Folyóirat szakterülete: Multidisciplinary helyzete: D1

Contents

Abbreviations

$[Cl^-]_e$: extracellular chloride ion
$[K^+]_e$: extracellular potassium ion
$[Na^+]_e$: extracellular sodium ion
2VO: 2-vessel occlusion (transient bilateral common carotid artery occlusion)
aCSF: artificial cerebrospinal fluid
ATP: Adenosine-tryphosphate
CBF: cerebral blood flow
$CMRO_2$: normal cerebral metabolic rate of oxygen
DC potential: direct current potential or slow cortical potential
DNA: Deoxyribonucleic acid
ECoG: electrocorticogram
EU: European Union
Green IOS: green intrinsic optical signal
LASCA: laser speckle contrast analysis
LED: light emitting diode
MABP: middle arterial blood pressure
N_2O: nitrous oxide
NO: nitric oxide
NR: Neutral Red
O_2: molecular oxygen
OEF: rate of oxygen extraction
PET: Positron emitted tomography
pHe: extracellular pH
pHi: intracellular pH
ROIs: regions of interest
SD: spreading depolarization
SHAM: sham-operated control
USA: United States of America

1. Introduction

1.1. Cerebral stroke; mechanisms of primary injury

Cerebrovascular diseases are ranked as the second leading cause of death after ischemic heart disease, because these cause nearly 10% of all death worldwide [1]. Devastating epidemiological data show that one in six people worldwide will have a stroke in their lifetime [2]. In addition, 15 million new stroke cases are reported in each year, and the consequences are mortal in half of the patients [2]. Based on the course of disease, stroke is caused by the interruption of constant cerebral blood flow (ischemic stroke) or the rupture of blood vessel(s) in the brain (hemorrhagic stroke). The incidence of ischemic stroke is much higher than hemorrhagic, it accounts for 87%-of all stroke cases [1]. Ischemic stroke occurs as a result of an obstruction of a cerebral artery that supplies a specific brain region. There are various sources and nature of the obstruction: (1) narrowing of vessel diameter due to atherosclerosis, (2) embolization: a fatty acid construct dissociates from the atherosclerotic plaque or an atrial fibrillation related thrombus develops and floats with circulation until it blocks a cerebral artery, (3) blockade of microvessels caused by the disturbances of the coagulation cascade. Two major zones of injury can be delineated around the ischemic focus (Fig. 1A); the ischemic core, which is the area of severe perfusion deficit (blood flow 10%-25%, <10 ml/l00 g/min) and the surrounding penumbra region (blood flow 30%-40%, approximately 15 to 40 ml/100 g/min), which consists of viable but non-functional tissue [3]. Vascular occlusion curtails the rate of oxygen extraction (OEF), depletes energy stores and causes necrosis of neurons and glia in the core [4]. The irrevocably damaged core region gradually expands at the expense of the penumbra, ultimately increasing lesions size and worsening neurological outcome [5].

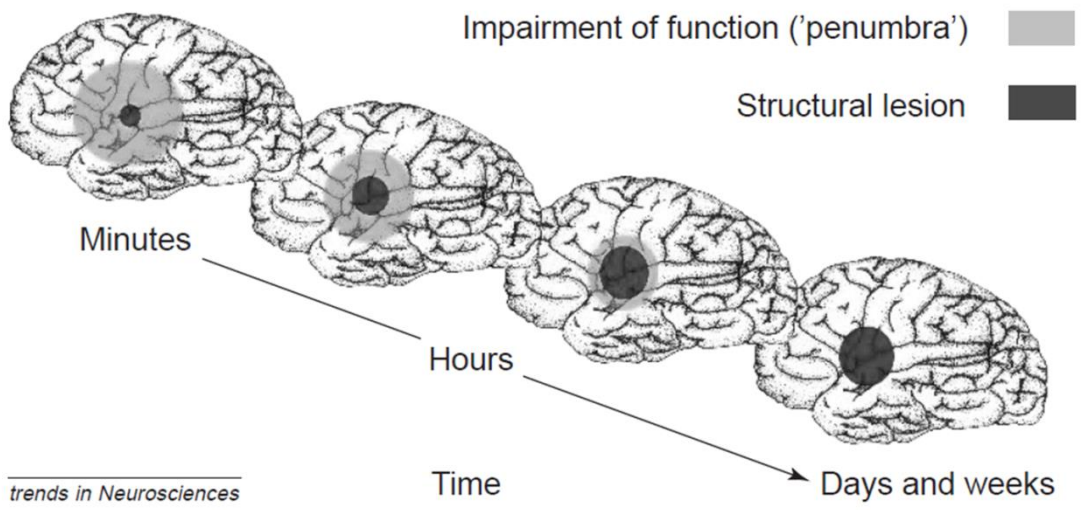

Figure 1. Schematic illustration of structural lesion growth in time (minutes, hours, days or weeks). In the early phase of ischemic stroke, clinical symptoms reflect the impairment of function (black). Over time, the expansion of core region recruits the functionally impaired but still viable penumbra region and deepens primary injury (Source: Dirnagl, Iadecola and Moskowitz, 1999).

The ischemic penumbra was defined as the portion of infarcted tissue around the core with reduced cerebral blood and absent electrical activity but preserved ion homeostasis [6]. Positron emitted tomography (PET) revealed that the gradual CBF reduction elevates the rate of oxygen extraction (OEF) to maintain the normal cerebral metabolic rate of oxygen ($CMRO_2$) in the penumbra [4]. Preserved energy metabolism leads to the failure of Na^+/K^+ pumps, increases the extracellular glutamate level and the receptor mediated intracellular calcium overload. Intracellular calcium accumulation participates in the formation of free radicals and the conversion of the vasodilator nitric oxide to the highly cytotoxic peroxynitrite [7]. The long-term diffusion of glutamate and potassium from the core to the penumbra mediates secondary pathological processes, such as the phenomenon of spreading depolarization (SD) that is thought to induce additional damage and contributes to the evolution of the ischemic lesions.

1.2. Typical features and injurious potential of spreading depolarization

Recurrent spreading depolarizations (SDs) spontaneously occur in the cerebral cortex for at least over a week after the surgical intervention for the alleviation of primary injury in subarachnoid hemorrhage, malignant stroke, and traumatic brain injury patients [8-10]. Furthermore, waves of SD were shown to evolve minutes after the onset of focal ischemia in the rat brain [11, 12]. The observation that SD appearance for days after the acute infarction was associated with delayed neurological deficits has led to promote SDs as causal biomarkers for the estimation of tissue metabolic failure in neurocritical care [13]. Finally, the inhibition of SD

occurrence in the injured brain of patients has been put forward as a therapeutic strategy to limit the expansion of primary lesions caused by hemorrhage or trauma [14].

Spreading depolarization is a slowly propagating wave of near complete sustained neural and glial depolarization followed by a temporary suppression of brain electrical activity. The main electrophysiological features of SD are the transient negative shift of the slow cortical or direct current (DC) potential and the silencing of neuronal activity after the passage of depolarization, the latter known as cortical spreading depression (Fig. 2). As the name implies, SD propagates over the nervous tissue, at a rate of 3-6 millimeters per minute, developing radially from a central point of origin in the cerebral grey matter. A sufficiently strong stimulus that is able to depolarize a critical volume of brain cells estimated to be ~1 mm^3 in the rat neocortex triggers SD [15]. The negative shift of the direct current (DC) potential is the hallmark of SD, which evolves parallel with ionic movements between the intra- and extracellular compartments: SD is accompanied by an increase of extracellular K^+ from 3–4 to 30–60 mM, and the concomitant decrease of the extracellular concentration of Na^+ from 140–150 to 50–70 mM and of Ca^{2+} from 1–1.5 to 0.2– 0.8 mM [16]. In addition to its prominent impact on brain ion homeostasis [17], SD induces fundamental metabolic changes in the tissue, reflected, for example, by the rapid consumption of glucose [18, 19], increased oxygen utilization [20, 21], reduction of tissue ATP content [19], accumulation of lactate [18, 22], and reduction of tissue pH [23].

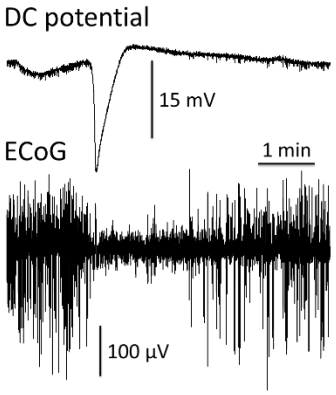

Figure 2. Electrophysiological features of spreading depolarization. Upper trace, negative shift of direct current (DC) potential, termed spreading depolarization (SD). Lower trace, transient suppression of the electrocorticogram (ECoG) called spreading depression of activity.

In the intact brain tissue, SD can be triggered experimentally by high-frequency electrical pulses ("tetanic" stimulation) or constant current stimulation ("galvanic"), mechanical stimuli such as needle pin prick or pressure application directly to the cortex, alkalotic pH, and a variety of chemicals [17]. The most widely used chemicals that reproducibly evoke SDs are K^+ ion, glutamate, ouabain and acetylcholine [17]. Experimental work proves, that SD is not harmful to the gross integrity of the nervous tissue under physiologic conditions [24].

In the injured brain, SDs generate spontaneously in an unpredictable manner in terms of space and time, due to severe oxygen deprivation, focal ischemic insults, or cerebral hypoperfusion -alone or in combination with hypotension [25]. These conditions that lead to metabolic failure and substrate supply-demand mismatch induce spontaneous waves of SD, which are suggested to start off at the border of ischemic foci called "periinfarct region" and propagate into the surrounding tissue [17]. Presumably, the interruption of constant oxygen and glucose supply deprives the energy consuming pumps (ATP-ases, secondary exchangers) of their substrates, and causes the accumulation of potassium and glutamate in the interstitial space, which lead to cellular depolarization and SD induction. The most serious consequence of the occurrence of recurrent SDs after focal ischemic stroke is the gradual conversion of viable but non-functional penumbra tissue into the irrevocably damaged core region, ultimately increasing lesion size and worsening neurological outcome [26]. The specific mediators of SD-related injury are not clear, but the insufficiency of the coupled cerebral blood flow response is an accepted contributor to the expansion of tissue damage.

1.3. The cerebral blood flow (CBF) response to spreading depolarization

SDs are currently believed to exacerbate ischemic brain injury via related atypical hemodynamic responses. Spreading depolarization generates a remarkable metabolic demand for oxygen and glucose because it strongly stimulates cellular ATP consumption. This need is met by increased local CBF. The hemodynamic response to SD consists of at least for sequential elements, which are achieved by a finely regulated balance between vasoconstriction and vasodilation [15]. In the intact brain, a short-lasting, initial vasoconstriction temporally coincides with the depolarization (i.e. the transient, negative DC shift indicative of SD) (Fig. 3A), and is known to become more pronounced under pathological conditions, such as ischemia [27]. The second and most conspicuous component is a profound CBF increase comparable to functional hyperemia of physiological neurovascular coupling, since it supplies the brain tissue with energy substrates to be used by ion exchange pumps for the restoration of resting membrane potential. This dominant hyperemic element emerges during the DC-repolarization and reaches the maximum amplitude after the DC shift recovery (Fig. 3 A,B) [15]. The third component of the CBF response is a slowly appearing, additional dilation setting in 3-5 min after SD, called late hyperemia (Fig.3A). Finally, a sustained phase of hypoperfusion evolves also known as post-SD oligemia that can last for up to an hour (Fig.3A). Interestingly, this concluding oligemic phase is typically associated with

the first SD in a train of SDs in naïve tissue, but cannot be discriminated with recurrent SDs that are elicited in a close temporal succession (i.e. at an inter SD interval of <30 min).

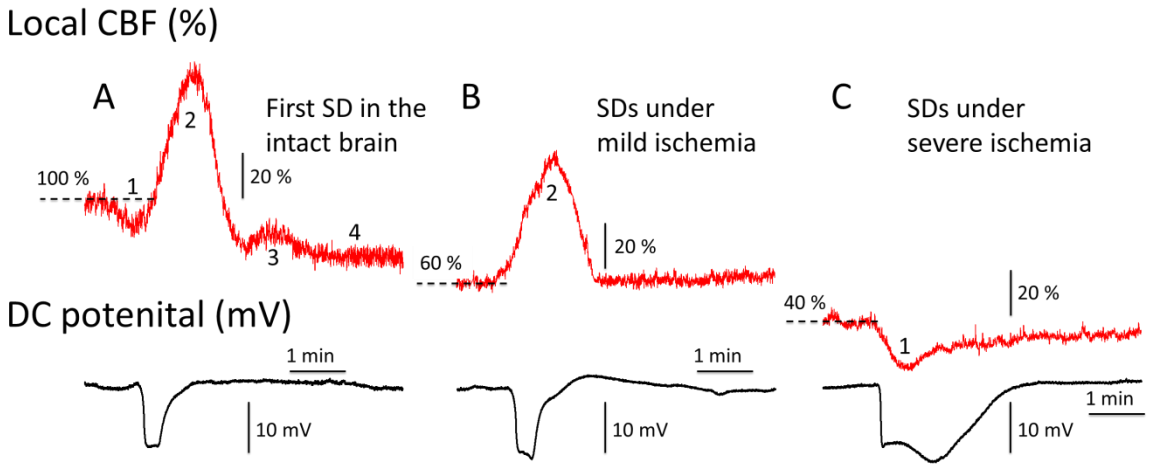

Figure 3. The representative traces illustrate that the kinetics of the local cerebral blood flow (CBF) response to spreading depolarization (SD) varies due to the metabolic status of the tissue. Lower black traces depict the negative direct current (DC) shift characteristic of SD; the upper red traces demonstrate the associated CBF response. A,Typical CBF response to the first evoked SD in the intact brain. All four, distinct elements of the CBF response occur including; (1) early hypoperfusion, (2) peak hyperemia, (3) late hyperemia and (4) long-lasting oligemia. B, Typical CBF response to recurrent, evoked SDs in the intact and mildly ischemic cortex. C, Domination and elongation of the early hypoperfusion (1) favors the occurrence of spreading ischemia in the severely ischemic cortex, in association with the elongation of DC shift duration.

Of the four separate CBF response components identified, the dominant hyperemic element evolves most reliably (Fig. 3B)., The different phases of the SD-related CBF response are assumed to be the result of a sequence and combination of extracellular ionic, neurotransmitter, and metabolic changes. It has been postulated that, similar to somatosensory activation, neurovascular coupling drives the hyperemic element of the SD-coupled CBF response [15].

In the injured brain, the CBF response to SD may undergo a gradual transformation to uncover ruling vasoconstrictive elements [28]. This transformation represents diminishing hyperemia synchronous with hypoemia becoming increasingly more obvious [29]. In the most severe form, the hypoemic element completely overrules hyperemia, which has become known as spreading ischemia (Fig. 3C), and is considered as a result of inverse neurovascular coupling [30]. This atypical CBF variation hampers the restoration of neural transmembrane potentials and causes the elongation of SD-related DC shift [31]. Prolonged SDs with spreading ischemia were recognized to produce the expansion of ischemic injury [28] and induce widespread necrosis in animals models [32].

1.4. Cerebral acidosis and the metabolic impact of spreading depolarization

A relevant, sensitive indicator of cellular metabolism is tissue pH, which is substantiated by the occurrence of a transient acidosis with neuronal activity [33]. Under pathological conditions such as global cerebral ischemia, brain regional lactic acidosis, secondary to accelerated anaerobic glycolysis, has been observed to directly impair cellular metabolism [34]. Excessive acidosis in the brain thus does not only designate altered metabolism, but has long been considered to cause neuronal injury possibly by generating free radicals, disrupting intracellular signal transduction pathways, and inducing DNA fragmentation [35]. Extracellular pH changes with SD contain a transient shift from 7.35 to 6.95 in the intact rodent cortex [23]. This relatively mild, brief acidosis by itself will not harm neurons, but could be crucial for neuronal loss or survival when repeatedly superimposed (i.e. recurrent SDs) on ischemia-induced acidosis characterized by pH values around 6.2-6.8 [36]. It is, therefore, reasonable to propose that there is indeed such an additive acid load, which would be an indicator of or, more importantly, a contributor to the SD-related metabolic crisis and related neurodegeneration in ischemic tissue. Direct measurement of tissue pH in the ischemic cortex has not been conducted to confirm or discard the validity of this concept, yet. Still, supportive experimental data have shown that lactate accumulation with SD is greater in the ischemic penumbra with respect to SDs propagating across the intact cortex [37].

1.5. Cerebral stroke, aging and spreading depolarization

Aging is associated with a progressive deterioration of function in all organs, including the brain. The brain heavily relies on a constant blood supply for its undisturbed function. During the physiological aging process, unfavorable changes occur in the brain's microcirculation, including increased vascular wall stiffness [38] decreased vascular density [39], impaired microvascular reactivity [40], and weakened remodeling potential [39]. The additive outcome is lower basal cerebral blood flow, but more importantly, reduced, suboptimal local cerebral blood flow elevation in response to neural activity. Degenerative diseases including those affecting the cerebrovascular system, are more common at older ages. Stroke is the third most common cause of death in Hungary and Europe, coming only after heart disease and cancer. Nearly three-quarters of all strokes occur in people over the age of sixty-five [41] and the risk of having a stroke more than doubles each decade after the age of fifty-five (Figure 4.). Even though stroke may occur in any phase of life, aging predicts poor patient outcomes while it

emerges as the most important independent risk factor for the incidence and prevalence of ischemic stroke [42].

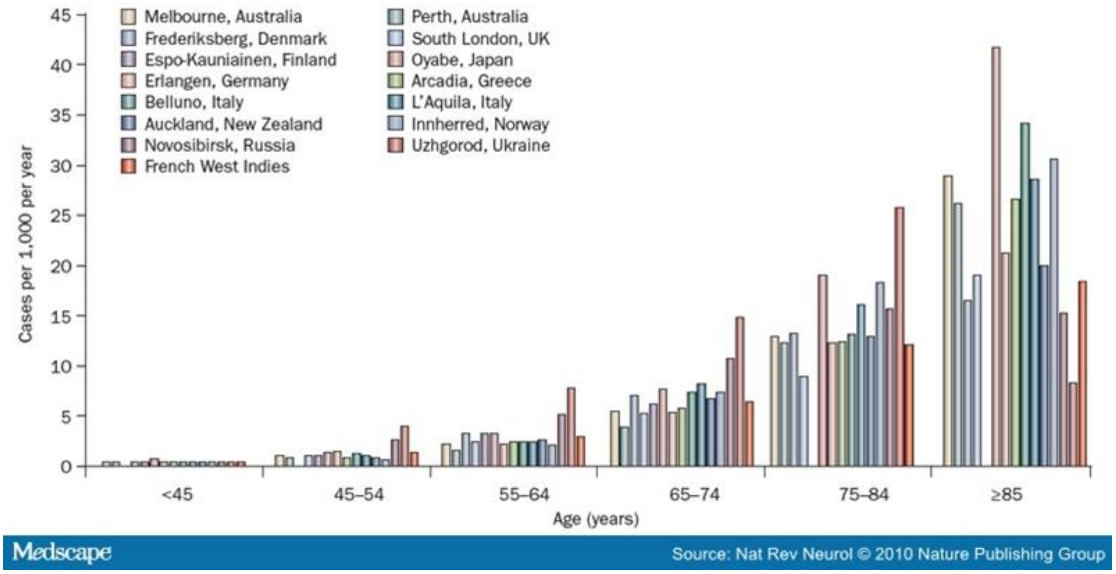

Figure 4. Incidence of stroke by age per 1000 population of all types of strokes admitted to clinical trial studies.

The impact of age on stroke pathophysiology has been the target of intensive research in order to understand the reason for the increased susceptibility of the aged brain to stroke-related injury. Aging was associated with the increased conversion of penumbra into infarction in patients [43], more severe ischemia-related neurological impairment in old mice, [42], and accelerated infarct development and neuronal degeneration in old rats [44]. Although SD may be implicated in all these events, the impact of aging on SD evolution, and the potential role SD might play in the age-related worsening of stroke outcome have remained largely unexplored [45]. Our group has recently made an important discovery that prolonged SDs and associated hypoperfusion likely compromise cortical tissue exposed to focal ischemia in aged rats [46].

1.6. Experimental hypotheses and aims of the study

Based on the above, we **hypothesized**, that;

(I) SDs are more injurious in the aged brain because the associated CBF response is impaired;

(II) The occurrence of recurrent SDs in the ischemic cortex is building up acid load to a level which has been recognized to cause tissue damage;

(III) The SD –related tissue acidosis is graver in the aged ischemic brain, which could contribute to more extensive ischemic lesions.

In order to prove the presented hypotheses, the following **aims** were formulated;

(I) To determine the impact of age on the evolution of SD and the kinetics of the associated changes in local CBF in the intact and ischemic rat brain.

We introduce an experimental model in which the degree of cerebral ischemia is highly reproducible, similar to the ischemic penumbra, and SDs can be elicited in a planned, controlled fashion. These conditions enable the accurate evaluation of how SD evolves in the old ischemic rat brain with respect to young control.

(II) To assess the degree of SD-related acidosis in the young and aged ischemic cortex of the rat, with respect to the intact condition.

To achieve the goals set, we relied on conventional pH-sensitive microelectrodes, and introduced tissue pH imaging. Even though pH-sensitive microelectrodes provide excellent extracellular pH (pHe) signal, additional, spatial resolution is also required to follow SDs that occur spontaneously at unpredictable sites in the ischemic cortex, and propagate across regions of various metabolic status. Neutral Red (NR) is a vital dye that indicates changes of intracellular pH (pHi) in the brain [47], and has been applied successfully to follow spatial patterns of activation, and spreading acidification and depression in the cerebellum [48, 49]. We adapted NR imaging to monitor pHi changes with SD in the rat cerebral cortex, and combined it with laser speckle contrast analysis (LASCA)-based cerebral blood flow (CBF) imaging to directly relate tissue pH changes to CBF variations.

2. Materials and methods

2.1. Surgical procedures

The experimental procedures were approved by the National Food Chain Safety and Animal Health Directorate of Csongrád County, Hungary. The procedures conformed to the guidelines of the Scientific Committee of Animal Experimentation of the Hungarian Academy of Sciences (updated Law and Regulations on Animal Protection: 40/2013. (II. 14.) Gov. of Hungary), following the EU Directive 2010/63/EU on the protection of animals used for scientific purposes, and reported in compliance with the ARRIVE guidelines.

Young adult (2 month-old, n=33) and old (18-20 month-old, n=18; 24 months old, n= 26) male Sprague-Dawley or Wistar rats were involved in two distinct subprojects (Experimental Project I and Experimental Project II) of the present study. Animals were anesthetized with halothane or isoflurane (1.5% - 2.2%, in N_2O:O_2/2:1) and allowed to breathe spontaneously through a head mask. Body temperature was kept between 37.1 °C and 37.3 °C using a heating pad, feedback controlled by a flexible rectal probe (Homeothermic Blanket System, Harvard Apparatus, Holliston, USA). The left femoral artery was cannulated for the continuous monitoring of mean arterial blood pressure (MABP; RX104A, TSD104A, Biopac Systems, Inc, Goleta, USA). Both common carotid arteries were exposed through a ventral cervical incision. A silicone-coated fishing line used as occluder was looped around each artery for later induction of acute, incomplete, global forebrain ischemia.

2.2. Experimental Project I

Male Sprague-Dawley or Wistar rats of 2 age groups (2-month-old, and 2-year-old, n=26) were involved. Animals were placed into a stereotactic frame, and 2 craniotomies were prepared on the right parietal bone (-3 mm caudal -5 mm lateral and -7 mm caudal -5 mm lateral from bregma) with a high precision dental drill (Technobox 810, Bien-Air Dental SA, Bienne, Switzerland). The dura in each craniotomy was carefully incised, and the craniotomies were regularly irrigated with physiological saline.

Ischemia induction was preceded by a 10-minute baseline period, during which all variables were continuously recorded (Fig. 5). Acute global forebrain ischemia was induced by pulling on the occluder lines looped around the common carotid arteries and securing them in place (“two-vessel occlusion”, 2VO) in a young and in an old group of rats (young 2VO, n=8; and old 2VO, n=6) (Fig. 5A). In an age-matched young group used as control for the surgical

procedures, the occluders were in place but not pulled on (young control, n=6) (Fig. 5B). For the old age-matched control group, acute 2VO was not implemented either; instead, animals had undergone permanent 2VO produced 1-year prior SD elicitation (old control, n=6). Recurrent SDs in all groups were triggered by placing a 1M KCl soaked cotton ball on the exposed cortical surface in the caudal cranial window 10 minutes after 2VO onset (Fig. 5). In old rats, 1M KCl often proved insufficient to trigger SD, therefore, either 3M KCl was used, or-if still inefficient-a tiny KCl crystal was placed on the cortical surface to achieve SD elicitation. Experiments were terminated by the overdose of the anesthetic agent.

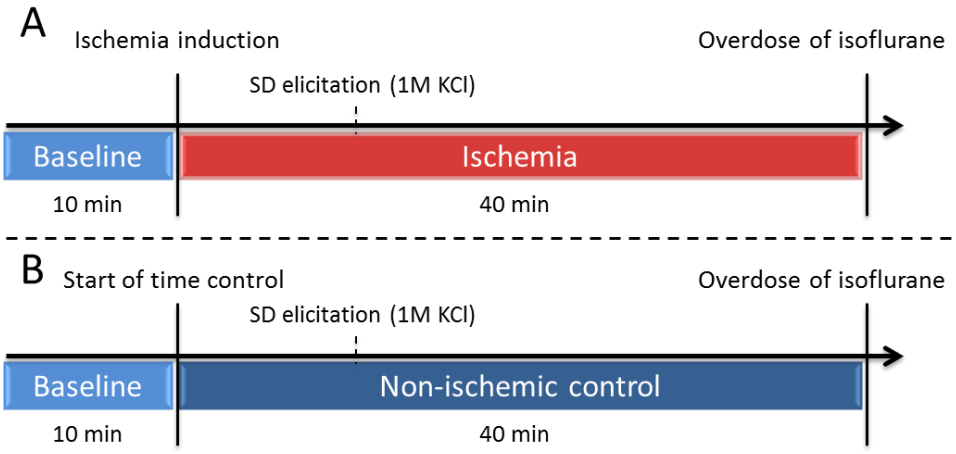

Figure 5. Schematic illustration of Experimental Protocol I. Panel A: After a 10 minute baseline global forebrain ischemia was induced by the permanent occlusion of both common carotid arteries ("two-vessel occlusion", 2VO). Panel B: Protocol for the age-matched SHAM operated and control animals. SDs were elicited 10 minutes after 2VO (Panel A) or 10 minutes after baseline acquisition (Panel B).

2.2.1. Recording of slow cortical or direct current (DC) potential

In the rostral craniotomy, slow cortical or direct current (DC) potential was acquired through a glass capillary electrode (20 μm outside tip diameter) filled with saline, implanted 1 - 1.2 mm deep into the cerebral cortex. An Ag/AgCl reference electrode was placed subcutaneously in the neck. DC potential was recorded via a high-input impedance preamplifier (NL102G, NeuroLog System, Digitimer Ltd Welwyn Garden City, Hertfordshire, England), connected to a differential amplifier (NL106, NeuroLog System, Digitimer Ltd) with associated filter and conditioner system (NL125, NL530, Digitimer Ltd, NeuroLog System). Potential line frequency noise (50 Hz) was removed by a high quality noise eliminator (HumBug, Quest Scientific Instruments Inc, North Vancouver, Canada) without any signal attenuation. Signals were acquired at a sampling frequency of 1 kHz. Analog to digital conversion was performed by a dedicated data acquisition system (MP 150, Biopac Systems, Inc). Data analysis was

assisted by the inbuilt instructions of the software AcqKnowledge 4.2 for MP 150 (Biopac Systems, Inc). For each SD, the amplitudes of depolarization and hyperpolarization were defined as the maximum of the negative and positive shift relative to baseline in DC potential, respectively and were expressed in mV. The maximum rates of depolarization and repolarization were calculated as the respective slopes of the SD-related DC shift given in mV/s. The duration of SD events was measured at half amplitude of the SD-related negative DC shift in seconds.

2.2.2. Monitoring of local CBF

SD-associated changes in local CBF adjacent to the glass capillary electrode were recorded by using laser-Doppler flowmetry (LDF). A stainless steel needle Doppler probe (Probe 403, connected to Periflux 5000, Perimed UK Ltd, Bury St Edmunds, UK) was positioned at an angle with a micromanipulator close to the penetration point of the glass capillary electrode. Care was taken to avoid large pial vessels. The LDF signal was digitized together with the DC potential as described above (MP 150, Biopac Systems, Inc). Six types of hemodynamic responses were identified, ranging from dominating hyperemia to prolonged cortical spreading ischemia with intermediate forms. The CBF response to each SD was classified accordingly, and the prevalence of various CBF response types was determined for each experimental group.

2.2.3. Data analysis

All variables (i.e., DC potential, LDF signal, and MABP) were simultaneously acquired, displayed live, and stored using a personal computer equipped with dedicated software (Acq-Knowledge 4.2 for MP 150, Biopac Systems, Inc). SD-associated relative changes in local CBF were calculated based on 100% baseline taken shortly before SD occurrence and residual LDF signal after anesthetic overdose considered as biological zero. The magnitude of each element of the SD-related CBF response (i.e., initial hypoperfusion, transient hyperemia, prolonged oligemia) was expressed relative to baseline (%). The duration of early hypoperfusion and subsequent transient hyperemia was measured at half amplitude of the initial hypoemic drop and hyperemic peak.

2.2.4. Statistics

Data are given as mean ± standard deviation for parametric data, and median (interquartile range 95%) for nonparametric data. The software SPSS (IBM SPSS Statistics for Windows, Version 20.0. Armonk, NY: IBM Corp) was used for statistical analysis. A one-way analysis

of variance (ANOVA) paradigm followed by a Fisher post hoc test was applied for the evaluation of data derived from the DC potential, and the duration of transient hyperemia. The prevalence of CBF response types across experimental groups was evaluated with the nonparametric Fisher's exact test. The magnitude of the elements of the CBF response and the SD-related changes were tested with repeated measures ANOVA. Correlation analysis between the duration of the SD-related negative shift in DC potential and transient hyperemia was performed with Spearman correlation analysis. Level of confidence was given as *$p < 0.05$ and **$p < 0.01$.

2.3. Experimental Project II

Young (2 month-old, n=20) and old (18-20 month-old, n=18) Sprague Dawley rats were used. After a 50 min long baseline, acute global forebrain ischemia was induced by 2VO (Fig. 6). An hour later, the carotid arteries were released to allow reperfusion of the forebrain for another hour. Experiments were terminated by the overdose of isoflurane. Three SDs were evoked with the topical application of 1M KCl during each phase of the experiments (i.e. baseline, ischemia and reperfusion) at an inter-SD interval of 15 minutes (Fig. 6). Samples for arterial blood gas analysis were withdrawn from the femoral artery before initiating the first SD, and under ischemia, before the release of the carotid arteries.

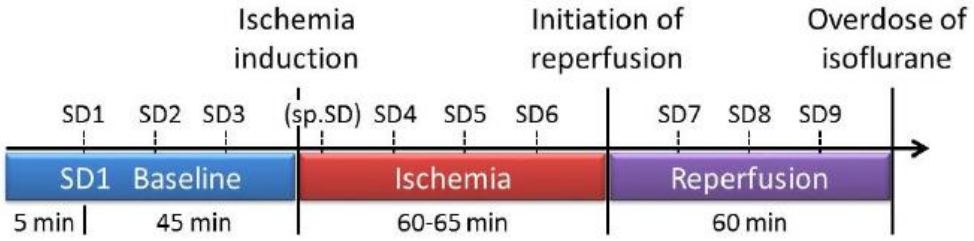

Figure 6. Schematic illustration of Experimental Protocol II. Numbered spreading depolarization events (e.g. SD1, SD2, … SD9) indicate SDs evoked by 1M KCl application. Spontaneous SD (sp.SD) evolved in some but not all experiments, and is given in brackets due to its inconsistent occurrence. Ischemia and reperfusion was induced by the occlusion and latter release of both common carotid arteries.

For tissue pH monitoring, the animals were assigned to either implantation of a pH-sensitive microelectrode into the cortex (n=17) (Fig. 7A), or a closed cranial window preparation over the parietal cortex for pH imaging (n=20) (Fig. 7B). The combination of the two approaches was successfully achieved in a representative case (Fig. 7C).

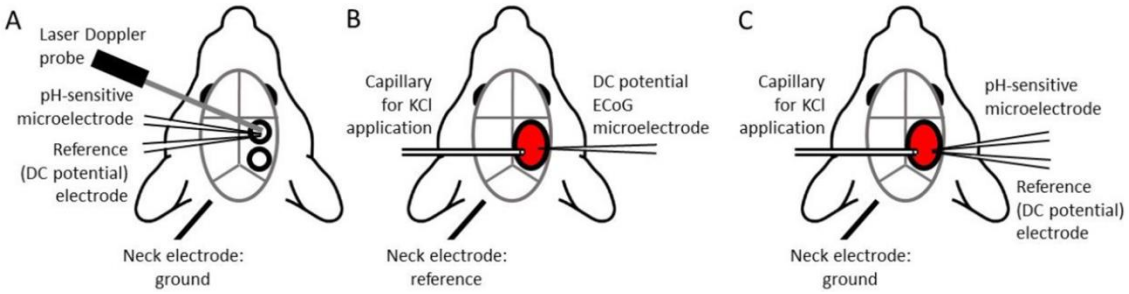

Figure 7. Experimental preparation for the various data acquisition protocols used. A, Conventional electrophysiological setting. Two open cranial windows were created (black circles) over the right parietal cortex. The frontal window served as recording site for data acquisition, and the caudal window was used for SD elicitation by the topical application of 1M KCl. B, Preparation for multimodal imaging (Neutral red fluorescence and laser speckle contrast analysis for the assessment of cerebral blood flow). A closed cranial window was built over the parietal cortex and subsequently loaded with Neutral red (black ellipse filled with red). The cranial window was equipped with a glass capillary to apply 1 µl of 1M KCl topically to elicit SD (left), and a glass capillary microelectrode to acquire direct current (DC) potential (right). C, Combination of multimodal imaging (shown in panel B) with conventional electrophysiology (shown in panel A).

2.3.1. Application of pH sensitive microelectrodes

Two craniotomies (5 mm apart) were prepared in the right parietal bone using a dental drill (Technobox, Bien Air 810) (Fig. 7A). The dura in each craniotomy was carefully dissected, and the craniotomies were regularly irrigated with artificial cerebrospinal fluid (aCSF; mM concentrations: 126.6 NaCl, 3 KCl, 1.5 $CaCl_2$, 1.2 MgCl, 24.5 $NaHCO_3$, 6.7 urea, 3.7 glucose bubbled with 95 % O_2 and 5 % CO_2 to achieve a constant pH of 7.4).

Ion-sensitive microelectrodes were prepared from glass capillaries pulled to obtain a tip diameter of 8-14 µm [50]. The capillaries were then silanized by exposure to N,N dimethyltrimethylsilylamine vapor (Sigma Aldrich) at 200 °C for 15 minutes. Subsequently, the capillaries were backfilled up to the shank with a solution containing 150 mM NaCl, 40 mM HEPES, and 20 mM NaOH. The electrode tip was immersed into a pH-sensitive liquid membrane solution (for exact composition see: [50]), to draw a membrane column of 80-250 µm into the tip of the electrode by gentle suction. Ion-sensitive microelectrodes were calibrated before and after each experiment using standard pH solutions (pH 6.11, pH 7.1 and pH 8.1). Voltage variations of 55-61 mV at 37 °C corresponded to 1 pH unit. Experiments were considered successful only when calibrations both before and after an experiment fell in the same range.

In each experiment, a pH-sensitive microelectrode was lowered with a micromanipulator 100-150 µm deep into the cortex, together with another glass capillary microelectrode (tip diameter=20 µm) filled with saline to serve as reference (n=17). The tips of the two electrodes were positioned as near as possible. The reference electrode acquired slow cortical or DC potential. An Ag/AgCl electrode was implanted under the skin of the animal's neck to be used

as common ground. Microelectrodes were connected to a custom-made dual-channel high input impedance electrometer (AD549LH, Analog Devices, Norwood, MA, USA) via Ag/AgCl leads. The voltage signal recorded by the reference electrode was subtracted from that of the pH-sensitive microelectrode by a dedicated differential preamplifier (NL834) and forwarded to an associated four channel analog signal isolator amplifier (NL 820), which yielded potential variations related to changes in H^+ ion concentration. The recorded signals were then forwarded to an analog-to-digital converter (MP 150, Biopac Systems, Inc) through filters (NL125) and conditioners (NL530). Electric signals via the electrodes were continuously acquired at a sampling frequency of 1 kHz, displayed live, and stored using a personal computer equipped with the software AcqKnowledge 4.2.0 (Biopac Systems Inc., USA). Extracellular pH (pHe) changes were expressed in mV to be translated into pH units offline, using least squares linear regression.

In order to assess changes in local CBF, a laser-Doppler needle probe (Probe 403 connected to PeriFlux 5000; Perimed AB, Sweden) was positioned at an angle adjacent to the intra-cortical microelectrode, avoiding any large pial vessels (n=14) (Fig. 7A). The laser-Doppler flow (LDF) signal was digitized and displayed together with the DC potential and pH signals as described above (MP 150 and AcqKnowledge 4.2.0, Biopac Systems, Inc. USA). The completed preparations were enclosed in a Faraday cage.

The caudal craniotomy was later used for SD elicitation by placing a 1M KCl-soaked cotton ball on the exposed cortical surface. The cotton ball was removed and the cranial window rinsed with aCSF immediately after each successful SD elicitation.

2.3.2. Neutral Red (NR) and cerebral blood flow imaging

A cranial window (4.5 × 4.5 mm) was opened with a dental drill over the parietal cortex. A doughnut-shaped ring of acrylic dental cement was mounted around the craniotomy, incorporating a perfusion inlet and outlet, and a glass capillary connected to a syringe pump (CMA/100, CMA/Microdialysis, Stockholm, Sweden) to be used to elicit SD by ejection of 1 µl 1 M KCl [51]. The chamber was filled with aCSF, and the dura carefully dissected before inserting an intra-cortical glass capillary microelectrode (outer tip diameter=20 µm) 800-1000 µm into the cortex near the lateral edge of the craniotomy, opposite to the site of later SD elicitation (Fig. 7B). The electrode was used to acquire DC potential, to confirm SD occurrence and propagation in the cortex. An Ag/AgCl electrode was implanted under the skin of the animal's neck to be used as reference. DC potential and ECoG were recorded via a high input impedance pre-amplifier (NL102G, NeuroLog System, Digitimer Ltd Welwyn

Garden City, Hertfordshire, England), connected to a differential amplifier (NL106, NeuroLog System, Digitimer Ltd, Welwyn Garden City, Hertfordshire, England) with associated filter and conditioner systems (NL125, NL530,Digitimer Ltd, NeuroLog System, Welwyn Garden City, Hertfordshire, England). Potential line frequency noise (50 Hz) was removed by a high quality noise eliminator (HumBug, Quest Scientific Instruments Inc., North Vancouver, Canada) without any signal attenuation. The cranial window was then sealed with a glass coverslip glued to the dental cement ring. The chamber was continuously perfused with aCSF at 25 µl/min using a peristaltic pump.

Neutral Red (3-amino-m-dimethylamino-2-methylphenazine hydrochloride, NR, Sigma-Aldrich), whose fluorescence intensity increases with decreasing pH was dissolved in saline (35 mM), and administered i.p. (2 x 1 ml) 30-35 min prior to the start of imaging to allow full saturation of the brain with the dye [47].

For live imaging, the cortex exposed by the cranial window was illuminated in stroboscopic mode (100 ms/s) with a high-power light emitting diode (LED) (530 nm peak wavelength; SLS-0304-A, Mightex Systems, Pleasanton, CA, USA) equipped with a bandpass filter (3RD 540-570 nm, Omega Optical Inc. Brattleboro, VT, USA). Emitted NR fluorescence passed through a 50 nm wide bandpass filter centered on 625 nm (XF3413-625QM50; Omega Optical Inc. Brattleboro, VT, USA), and was captured with a monochrome CCD camera (resolution: 1024 × 1024 pixel, Pantera 1M30, DALSA, Gröbenzell, Germany) attached to a stereomicroscope (MZ12.5, Leica Microsystems, Wetzlar, Germany). The stereomicroscope was equipped with a 1:1 binocular/video-tube beam splitter to allow the mounting of a second camera. The captured NR images were enhanced by 2 × 2 software binning to increase the sensitivity of the NR fluorescence detection. Image resolution after binning was reset to the original 1024 × 1024 pixels. Synchronous with NR images, green intrinsic optical signal (IOS) was captured at 100 ms exposure each second by the second CCD camera identical to that used for NR imaging, but with no emission filter. Green IOS was later used for anatomical orientation, and NR signal correction. In addition, both cameras recorded background (i.e. potential incident light and noise of the camera chip) at 1 frame per second frequency, to be used for the correction of raw images. The overall magnification of the images was × 3.15 and the size of the field of view was 3.8 × 3.8 mm. A dedicated program written in LabVIEW environment synchronized the illumination and camera exposures. Finally, NR fluorescence was mathematically corrected offline, for the absorption of excitation and fluorescence wavelengths by hemoglobin [52], and for the bleaching of NR.

NR imaging was combined with CBF imaging involving laser speckle contrast analysis (LASCA), [53]. The cortical area exposed by the cranial window was illuminated with a laser diode (HL6545MG, Thorlabs Inc., New Jersey, USA; 120 mW; 660 nm emission wavelength) driven by a power supply (LDTC0520, Wavelength Electronics, Inc., Bozeman, USA) set to deliver a 160-mA current. The raw laser speckle images were captured by the second CCD camera. Laser illumination and camera exposure were synchronized (1 frame/second; 2 ms for illumination and 100 ms for exposure). Image processing was carried out in MATLAB (The MathWorks Inc., Natick, MA, USA). Briefly, CBF maps were computed from the corresponding raw images [54], following the reduction of background noise by subtracting the local variance and local mean values of the background images from the corresponding raw speckle images.

Local changes in NR fluorescence intensity and CBF with time were extracted by placing regions of interest (ROIs) of 19 × 19 pixel size (~70 × 70 μm) at selected sites devoid of any blood vessels visible in the images. Identical ROIs were applied on the NR and CBF image sequences acquired simultaneously.

2.3.3. Data analysis

Data analysis was assisted by the inbuilt tools of the software AcqKnowledge 4.2 (Biopac Systems, Inc., USA), or was transferred into a MATLAB environment (The MathWorks Inc., Natick, MA, USA). The DC potential, pH and LDF signals were first downsampled to 1 Hz. To assess pH variations with SD quantitatively, we analyzed in detail the dominating acidosis obvious on the pH signature of SD acquired with both pH sensitive microelectrodes and NR imaging. The following variables were measured: amplitude and duration of acidosis at half amplitude, magnitude of acidosis expressed as area under the curve, the slope of acidosis and recovery from acidosis, and tissue pH 12 min after each SD.

CBF recordings obtained by LDF or LASCA were expressed relative to baseline by using the average CBF value of the first 240 s of baseline (100%) and the recorded biological zero obtained after terminating each experiment (0%) as reference points. Elements of the SD-related CBF response were characterized as follows: amplitude and duration of early hypoperfusion, amplitude and duration of hyperemia, and magnitude of hyperemia (area under the curve).

SDs were divided into two major categories based on whether the event was triggered with KCl (evoked SDs), or occurred due to the induction of ischemia (spontaneous SDs). Evoked SDs were further subdivided into first SD (SD1), subsequent SDs during baseline, SDs under

ischemia, and SDs during reperfusion. The impact of age was evaluated for both evoked and spontaneous SDs. SDs that were identified on DC potential traces as negative shifts with an amplitude less than 5 mV were termed as “mini” SDs, and were evaluated in young animals with respect to normal SDs (i.e. the negative DC shift greater than 5 mV).

2.3.4. Statistics

Data are given as mean±stdev. The software SPSS (IBM SPSS Statistics for Windows, Version 22.0, IBM Corp.) was used for statistical analysis. A two-way analysis of variance (ANOVA) paradigm considering age and the phase of the experiment as its factors was applied for the evaluation of tissue pH variations with SDs, the SD-related hemodynamic variables. Level of significance for the ANOVA was defined as $p<0.05$* and $p<0.01$**. Significant differences between groups were determined by a Fisher post hoc test as follows: $p^{*}<0.05$ and $p^{**}<0.01$, vs. respective Baseline; $p^{+}<0.05$ and $p^{++}<0.01$, vs. respective Ischemia; $p^{\#}<0.05$ and $p^{\#\#}<0.01$, vs. respective Young.

Tissue pH changes with the first SDs were analysed relying on the repeated measures ANOVA paradigm (F value is given in each plot, levels of significance were determined as $p<0.05$* and $p<0.01$**) followed by pairwise comparisons ($p<0.05$* and $p<0.01$** vs. prior to SD1; $p<0.01^{\#\#}$ vs. prior to SD2). Correlation analysis between the amplitude of SD-related acidosis and the duration of hyperemia was tested by Pearson one-tailed correlation analysis ($p<0.01$**).

3. Results

3.1. Experimental Project I.

3.1.1. The DC potential signature of spreading depolarization

The approach of SD elicitation (i.e., placing a KCl-soaked cotton ball on the exposed cortical surface) induced recurrent SDs at irregular intervals. In the young groups, SD elicitation with the topical application of 1M KCl was successful in each experiment; by contrast, 1M concentration of KCl was insufficient to trigger SD in the old groups - instead, 3M KCl or, when still ineffective, a small KCl crystal was required for SD generation, indicative of a higher elicitation threshold for SD in the old animals.

SDs were transient (i.e., transient negative shifts in the DC potential, Fig. 8A), except for 1 animal in the old 2VO group, in which the first SD appeared to be terminal (i.e., no recovery of the DC potential till the termination of the experiment). In general, 2 - 3 SDs were recorded

in the young 2VO and old 2VO groups during ischemia, in contrast with 4 - 5 SDs in the respective nonischemic control groups, showing a tendency for lower SD frequency during ischemia.

Because recurrent SDs occurred at irregular intervals, often in a rapid succession that disabled the reliable analysis of the CBF responses associated with subsequent SDs, the first SD alone was analyzed comprehensively. As Fig. 8A demonstrates, the most obvious effect of ischemia was the elongated duration of the SD related negative DC shift (e.g., 66.2 ± 22.8 vs. 21.4 ± 4.1 seconds, young 2VO vs. young control; Fig. 8B), which was augmented further by age as seen in the old 2VO group (95.8 ± 46.2 seconds, Fig. 8B). The ischemia-related, elongated duration of SDs was also reflected in the reduced slopes of depolarization (14.5 ± 11.4 vs. 4.4 ± 2.9 mV/s, young 2VO vs. young control; Fig. 8C) and repolarization (0.7 ± 0.5 vs. 2.6 ± 0.7 mV/s, young 2VO vs. young control; Fig. 8D). Old age was associated with a reduced slope of depolarization, as well (1.9 ± 0.9 vs. 2.6 ± 0.7 mV/s, old control vs. young control; Fig. 8C). Finally, the amplitude of depolarization and repolarization tended to be smaller in the ischemic groups (Fig. 8E and F), and older age was associated with a reduced amplitude of repolarization (2.9 ± 2.9 vs. 5.1 ± 1.2 mV, old control vs. young control; Fig. 8F).

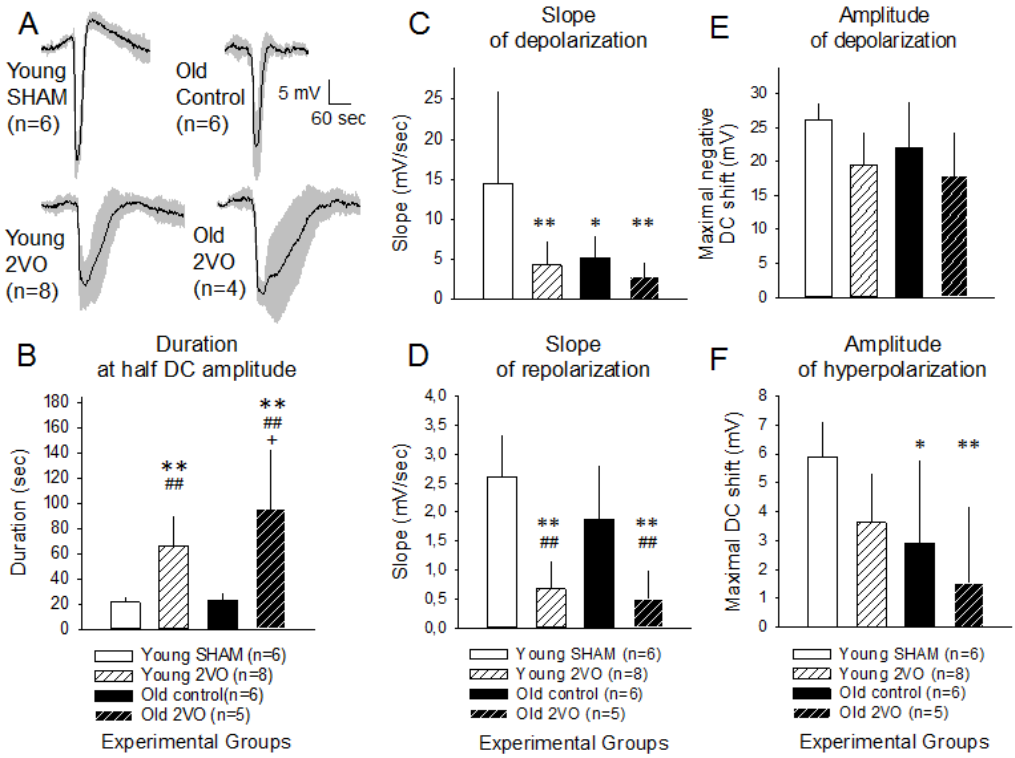

Figure 8. Age- and ischemia-related changes in the direct current (DC) potential signature of first evoked spreading depolarization (SD1) in each experiment. (A) Traces of SD-related negative DC shifts (mean±stdev) for each experimental group; (B) Duration of SD measured at half amplitude of the negative DC shifts; (C) Amplitude of the SD-related depolarization given as the maximum negative DC shift with respect to baseline; (D) Amplitude of the SD-related hyperpolarization measured as the maximum positive DC shift during repolarization with respect to baseline (E) Maximum rate of depolarization determined as the slope of the negative DC shift; (F) Maximum rate of repolarization calculated as the slope of the positive DC shift. All data are given as mean±stdev. A one-way analysis of variance (ANOVA) paradigm followed by a Fisher post hoc test was applied for statistical analysis. Levels of significance are given as *P<0.05, **P<0.01 vs. Young SHAM, #P<0.05, ##P<0.01 vs. Old control, +P<0.05 vs. Young 2VO. Abbreviations: 2VO, 2-vessel occlusion (transient bilateral common carotid artery occlusion); SHAM, sham-operated control.

3.1.2. Laser-Doppler recording of CBF response to spreading depolarization

Ischemia induction by 2VO caused a marked drop of CBF in the young 2VO and old 2VO groups to 41 ± 9.4% and 38 ± 18.2% of baseline, respectively. In contrast, CBF taken at the end of the ischemic period persisted at 43 ± 22.1% in the young 2VO group, but decreased further to 18 ± 13.6% in the old 2VO group, being significantly lower than CBF in the same group earlier at ischemia onset ($p < 0.024$), or CBF in the young 2VO group at the end of ischemia ($p < 0.028$). Finally, CBF peaked during reperfusion at 83 ± 27.6% and 106 ± 62.1% in the young 2VO and old 2VO groups, respectively, with no statistically significant difference due to age ($p < 0.366$). No CBF variation was observed throughout the experimental period in the control groups.

Screening all experimental groups and all SDs elicited, 6 types of SD-associated CBF response were determined based on the kinetics of their laser-Doppler trace. As shown in Figure 9A, the CBF response types were ranked from the physiological types (Type 1 and Type 2) toward those consisting of a decreasing hyperemic and more obvious hypoemic component (Types 3-5), ending with spreading ischemia (Type 6). In addition, a few SDs occurred without a detectable variation in CBF (i.e., no CBF response). Because the most important parameter in the spectrum from normal hyperemic responses to inverse responses is the increasing duration of the initial hypoperfusion [28, 55], its duration was quantified (table in Fig. $9B_{(1)}$). As expected, early hypoperfusion was increasingly more represented with higher rank CBF response types. Next, the distribution of the defined CBF response types associated with the first SD was evaluated across experimental groups (Fig. $9B_{(2)}$). The young control group displayed only the physiological Type 1 (n = 4/6) and Type 2 (n = 2/6) responses, while the first SD in the young 2VO animals was coupled with Types 3 - 5 response, Type 4 being the most frequent of all (n = 5/8). The old control group developed a wide spectrum of CBF responses ranging between Types 1 - 4, including an animal with no CBF response, which displayed an age-related shift to higher rank types as compared with the young control group. The first SDs in the old 2VO group were associated with either Type 4 (n = 2/6) or Type 6 (n = 4/6) CBF response, showing a striking share of spreading ischemia (i.e., Type 6). Quantitative analysis of the duration of early hypoperfusion (table in Fig. $9B_{(2)}$) indicated that this first element of the CBF response to SD was elongated during ischemia (36.8 ± 17.5 vs. 7.9 ± 6.8 seconds, young 2VO vs. young control) and became drastically longer in the old 2VO group (1344 ± 1047 seconds), due to the prevalence of spreading ischemia.

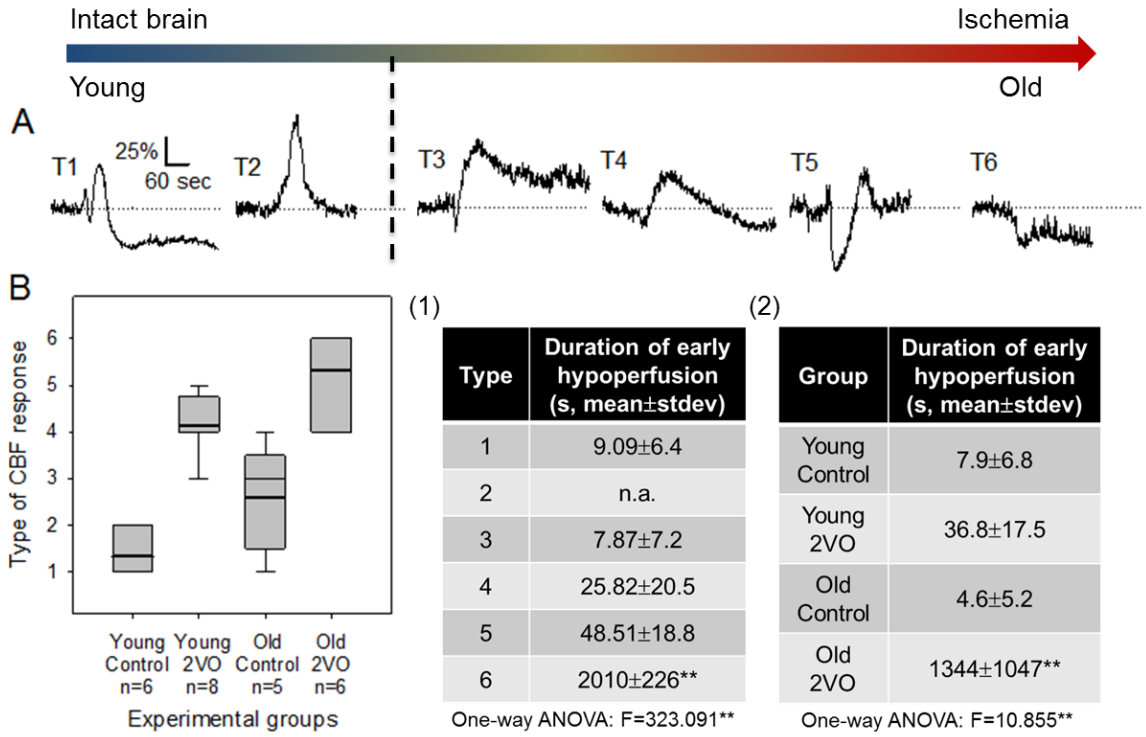

Type	Duration of early hypoperfusion (s, mean±stdev)
1	9.09±6.4
2	n.a.
3	7.87±7.2
4	25.82±20.5
5	48.51±18.8
6	2010±226**

Group	Duration of early hypoperfusion (s, mean±stdev)
Young Control	7.9±6.8
Young 2VO	36.8±17.5
Old Control	4.6±5.2
Old 2VO	1344±1047**

Figure 9. Various kinetics of the spreading depolarization related cerebral blood flow (CBF) response. (A) Types of detectable CBF response associated with SD events. Each type is demonstrated by a representative trace. CBF responses were ranked from the physiological types toward those consisting of a decreasing hyperemic and more obvious hypoemic component. Shaded arrow (top) shows the transformation spectra of the CBF response. Broken line separates intact CBF response types from the effects of ischemia and aging. (B) Distribution of the defined types of CBF response across experimental groups. The box plot displays data for the first SD (SD1). Data were evaluated with the nonparametric Fisher's exact test. Level of confidence was determined as **p < 0.001. The table (1) in panel B displays the mean duration of early hypoperfusion (i.e., hypoemic component) for each type, to indicate the progressively increasing share of hypoperfusion in the full CBF response (**p < 0.001, Type 6 vs. Type 1). The table (2) in panel B shows the mean duration of early hypoperfusion (i.e., hypoemic component) for each experimental group (**p < 0.001, old 2VO vs. all other groups). Abbreviations: ANOVA, analysis of variance; CBF, cerebral blood flow; control, sham operated control, stdev, standard deviation; 2VO, 2-vessel occlusion (bilateral common carotid artery occlusion).

The quantitative analysis (Fig. 10) relying on the hyperemic Type 1 - 5 CBF responses (i.e., those containing a transient hyperemic element) revealed that ischemia reduced the amplitude of hyperemia in both young (57 ± 10.1 vs. 156 ± 47.7%, young 2VO vs. young control) and old animals (30 ± 17.9 vs. 181 ± 72.7%, old 2VO vs. old control). At the same time, ischemia extended the duration of hyperemia significantly (237 ± 97 vs. 37 ± 12 seconds, young 2VO vs. young control; 122 ± 75 vs. 46 ± 14, old 2VO vs. old control). Taken together, the hyperemic CBF responses to SDs were of smaller amplitude but longer duration under ischemia.

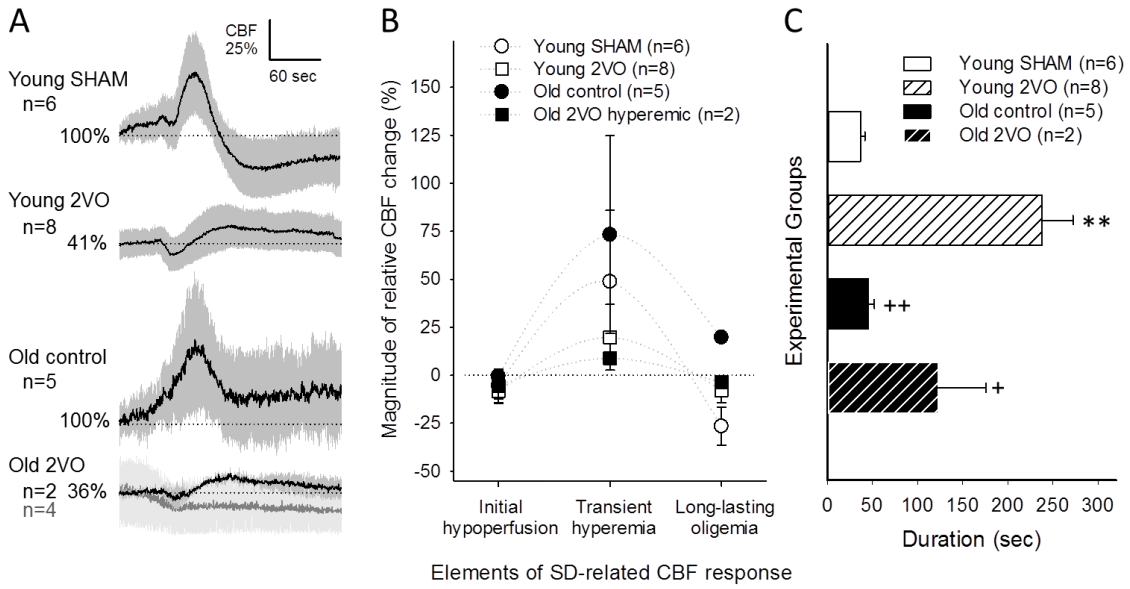

Figure 10. Quantitative evaluation of the cerebral blood flow (CBF) response coupled with the first spreading depolarization (SD) event in each experiment. (A) Average CBF response (mean±stdev) illustrated for each experimental group. Horizontal dotted lines indicate mean CBF (%) prior to SD elicitation. In the Old 2VO group, hypoemic CBF response was detected in 4 of the 6 animals (gray trace). (B) Magnitude of the three distinct elements of the SD-associated CBF response (mean±stdev). Repeated measures ANOVA was used for statistical analysis (group effect: **$p<0.003$). A Fisher post hoc test revealed a significant difference in the kinetics of the CBF response in the Young 2VO and Old 2VO groups with respect to the Young SHAM group (**$p<0.002$). The difference between the Old control and Old 2VO groups was also nearly significant ($p<0.057$). (C) Duration of transient hyperemia (mean±stdev). A one-way ANOVA paradigm followed by a Fisher post hoc test was applied for statistical analysis. Levels of confidence were determined as **$p<0.001$ vs. Young SHAM, +$p<0.05$ and ++$p<0.001$ vs. Young 2VO. Abbreviations: 2VO, 2-vessel occlusion (transient bilateral common carotid artery occlusion); SHAM, sham-operated control.

3.2 Experimental Project II.

3.2.1. Mean arterial blood pressure and blood gases in the ischemia model used

Key actors in body pH regulation are the lungs which control the partial pressure of CO_2 in the blood and the kidneys which regulate the levels of the other important acid–base species, especially HCO_3^- [56]. Since brain pH is highly influenced by the metabolic status of the peripheral organs, we regularly measured the arterial blood gases of animals. Mean arterial blood pressure (MABP) was similar in the two age groups, but elevated significantly during ischemia (103.9±12.1 vs. 94.2±13.3 mmHg, ischemia vs. baseline), and returned to pre-ischemic values during reperfusion (96.0±9.8 vs. 94.2±13.3 mmHg, reperfusion vs. baseline). The data obtained by arterial blood gas analysis are summarized in Table 1. Blood pH proved to be more alkaline in the old animals with respect to the young during baseline (pH 7.40±0.02 vs. 7.37±0.03, old vs. young) in the face of similar pCO_2 (34.69±5.1 and 34.66±5.4 mmHg, old and young), slightly elevated HCO_3^- (21.61±3.0 vs. 20.13±3.1 mmol/l, old vs. young), and significantly lower lactate concentration (0.71±0.2 vs. 0.80±0.3 mmol/l, old vs.

young). During ischemia, blood pH decreased in the young (pH 7.34±0.05 vs. 7.37±0.03, ischemia vs. baseline) but increased in the old animals (pH 7.43±0.04 vs. 7.40±0.02, ischemia vs. baseline). The level of HCO_3^- was higher in both age groups during ischemia, as compared to baseline (young: 22.23±3.2 vs. 20.13±3.1 mmol/l; old: 23.28±3.7 vs. 21.61±3.0 mmol/l; ischemia vs. baseline).

Table 1. Obtained values and statistical evaluation of arterial blood pH, and the level of metabolites relevant for pH adjustment in arterial blood.

Variable	Phase of experiment	Age		Multivariate analysis (factors)			
		Young (n=16)	Old (n=19)	Stat. values	Ischemia	Age	Ischemia x Age
pH	Baseline	7.37±0.03	7.40±0.02	F	0	48.05	11.85
	Ischemia	7.34±0.05	7.43±0.04	p	0.983	0.0001**	0.001**
pCO_2	Baseline	34.66±5.4	34.69±5.1	F	4.204	4.435	4.506
	Ischemia	41.34±8.2	34.57±7.6	p	0.044*	0.039*	0.038*
HCO_3^-	Baseline	20.13±3.1	21.61±3.0	F	5.846	2.632	0.073
	Ischemia	22.23±3.2	23.28±3.7	p	0.018 *	0.109	0.788
Lactate (mmol/l)	Baseline	0.80±0.3	0.71±0.2	F	1.247	5.113	0.499
	Ischemia	0.90±0.3	0.74±0.2	p	0.268	0.027*	0.482

Data from both the Electrophysiology and Imaging series of experiments are shown. Level of significance is given as $p<0.05$* and $p<0.01$**.

3.2.2. Tissue pH imaging using Neutral Red with reference to pH-sensitive microelectrodes

Tissue pH imaging relied on the increasing fluorescence intensity of NR with decreasing pH values [47]. The imaging approach has been introduced to allow the assessment of the spatio-temporal dynamics of tissue pH variations associated with SD, the spatial resolution being a significant additional aspect as compared with pH-sensitive microelectrodes. An important difference between pH-sensitive microelectrodes and NR imaging, however, is the source of the tissue pH signal, which is extracellular for microelectrodes [50], and primarily intracellular for NR imaging [47].

In all experiments, each SD in the intact and ischemic cortex was accompanied by a highly reproducible, transient elevation of NR fluorescence intensity, which was somewhat diffuse (i.e. no sharp wave front), but propagated across the field of view discernably from the site of SD elicitation in a radial fashion (Fig. 11). The captured pH transients were undoubtedly related to SDs as confirmed by the typical negative DC shift and the simultaneous depression of the ECoG recorded by an intra-cortical microelectrode positioned distant to the site of SD

elicitation (Fig. 11). Furthermore, the propagation of the NR fluorescence intensity elevation was spatially and temporally locked with the SD-coupled CBF response visualized by LASCA (Fig. 11), and the advancing, sharp wave front designating SD in green IOS image sequences.

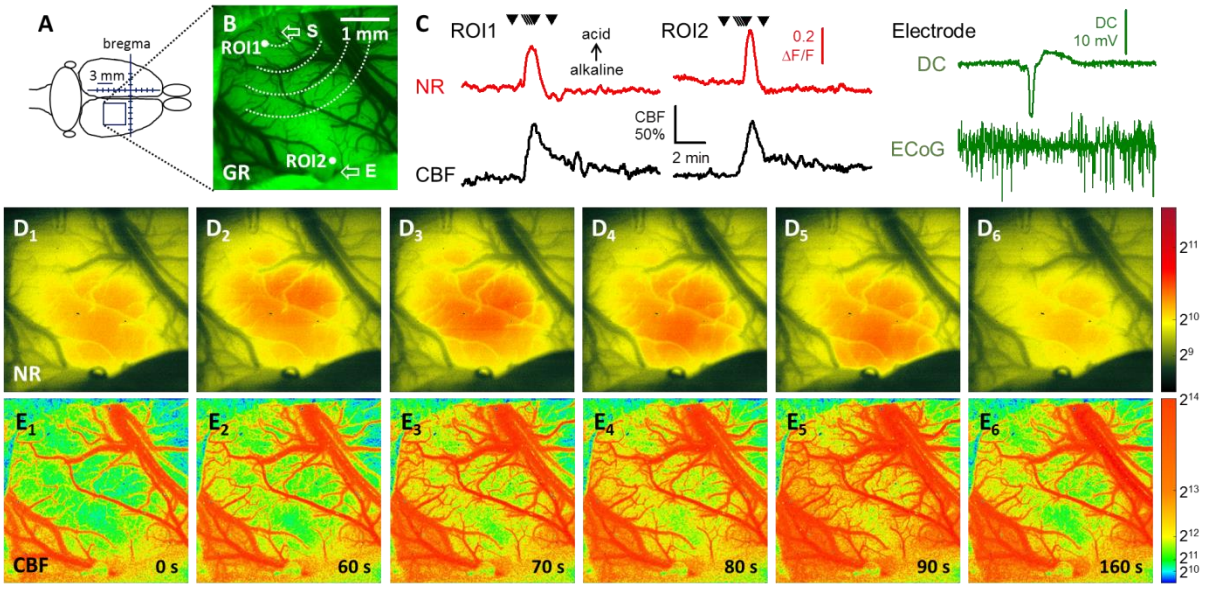

Figure 11. Representative raw image sequences and graphs displaying relative variations illustrate synchronous changes in Neutral Red (NR) fluorescence, cerebral blood flow (CBF), direct current (DC) potential and the electrocorticogram (ECoG) with the propagation of a spreading depolarization (SD) wave in the intact cerebral cortex of a young rat. A, Position of the closed cranial window over the parietal cortex; B, The cortical surface at green light illumination. Two regions of interest (ROI) indicate the origin of NR and CBF traces shown in Panel C. The tip of the capillary used to trigger SD (S), and the penetration site of the glass capillary electrode (E) inserted to acquire electrophysiological signals are shown with arrows. C, Traces demonstrate SD-related relative changes in NR fluorescence (red) and CBF (black). The occurrence of SD was confirmed by the negative shift of the DC potential and the transient depression of the ECoG (green). Small black triangles pointing down over the NR traces designate the origin of the representative images shown in Panels D-E. D, Pseudo-colored images of NR fluorescence demonstrate a propagating increase of fluorescence intensity associated with SD; the original images relying on a 16-bit grayscale. A scale bar to the right represents the used color range. E, Pseudo-colored perfusion maps based on laser speckle contrast images show the CBF response with SD, and display speckle contrast perfusion units. Warmer colors represent higher CBF. A scale bar to the right represents the used ranges of gray levels.

The pH-sensitive microelectrodes applied in our study revealed three subsequent phases of pHe variations associated with SD: (i) a brief, initial acidic shift immediately followed by (ii) a rapid, short alkaline shift, and (iii) a final, longer-lasting, dominant, transient acidosis (Fig. 12A, blue trace). The latter, dominant acidosis has become the focus of our quantitative data analysis.

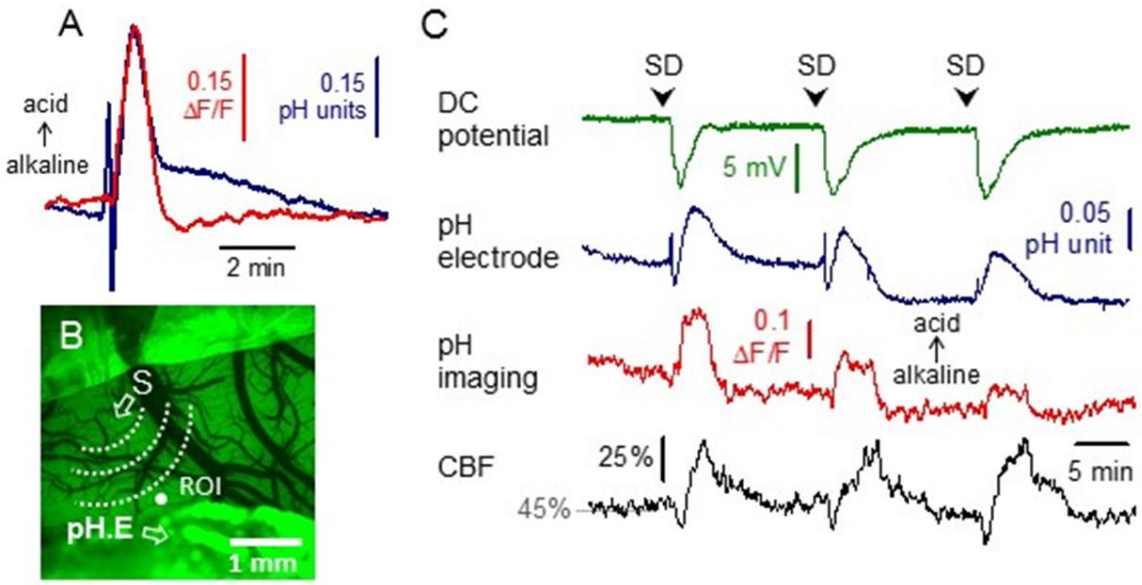

Figure 12. Changes in Neutral Red (NR) fluorescence indicate tissue pH variations with spreading depolarization (SD) and are correlated with the signature of SD acquired with pH-sensitive microelectrodes. A, Overlay of traces recorded with pH-sensitive microelectrodes (blue) and imaging of Neutral Red fluorescence (red), taken during the propagation of recurrent SD waves in the intact cortex of young rats. Note that acidosis (decreasing pH) is depicted upward. Each trace is the mean of individual events (SD2) obtained from separate experiments (n=6). B, A field of view revealed by the cranial window at green light illumination. A region of interest (ROI) indicates the origin of NR and cerebral blood flow (CBF) traces shown in panel C. Note the tip of the capillary used to trigger SD (S), and the position of the pH sensitive and reference electrodes (pH.E) inserted into the cortex to acquire local changes in tissue pH and direct current (DC) potential. C, Synchronous traces obtained during ischemia from the cranial window of a young rat shown in panel B. Note the good correspondence of pH signals acquired with a pH-sensitive microelectrode (blue) and NR imaging (red). The DC potential trace (green) confirms SD occurrence.

The kinetics of the increase of NR fluorescence intensity with each SD was comparable to that of the dominant tissue acidosis acquired with pH-sensitive microelectrodes (Fig. 12). In particular, the duration of this marked acidosis measured at half amplitude was nearly identical as assessed with the two distinct methods (for baseline SDs in young rats, pH-sensitive microelectrode: 40.2±8.1 s, NR imaging: 39.8±13.8 s). However, the initial, brief acidic and subsequent alkaline shifts obvious on the pH-sensitive microelectrode signal (Fig. 12A, blue trace) did not appear consistently on the traces obtained with NR imaging (Fig. 12A, red trace). Finally, the recovery from SD-related acidosis as acquired by microelectrodes seemed to contain an additional, slow component responsible for a more gradual recovery of pHe, which did not occur on the pHi signature of SD provided by NR imaging (Fig. 12).

A clear limitation of NR imaging concerned the late phase of the experiments. During reperfusion, NR imaging failed to expose SD-related pHi changes reliably (the amplitude of NR fluorescence intensity elevation was very small, if any) (Fig. 13), despite of the consistent DC signature of and CBF response to SDs. This was most certainly caused by the exhaustion of the dye. This perception was supported by the negligible increase of NR fluorescence

intensity with SDs triggered in the intact cortex over 2 hours after the start of imaging, with no prior ischemia or SD elicitation (Fig. 13B). In contrast, pH-sensitive microelectrodes provided good quality pHe signals with SDs during the phase of reperfusion, similar to SD-related pH transients recorded in the intact cortex under baseline conditions (Fig. 13A).

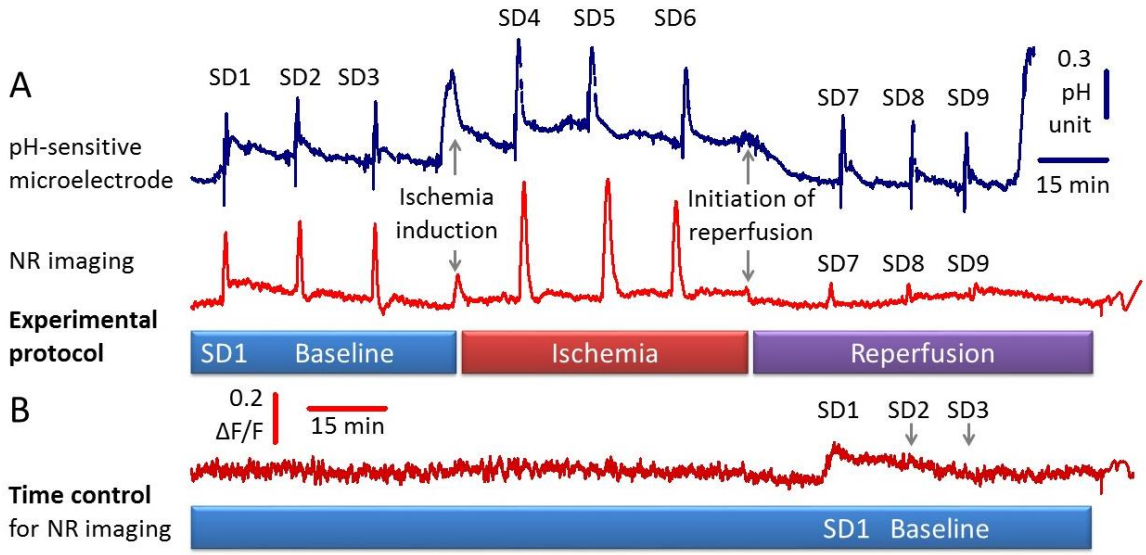

Figure 13. Representative traces acquired with pH-sensitive microelectrode (blue) and Neutral red (NR) imaging (red), corresponding to the subsequent phases of the experimental protocol (A) and time control experiments (B). Note that NR imaging does not provide reliable pH signal by the late phase (i.e. corresponding to the phase of reperfusion of the experimental protocol) of experiments.

3.5. Various kinetics of pH transients with spreading depolarization in the intact cortex

For recurrent SDs triggered in the rat intact cortex as presented here, it has been shown repeatedly that the final, long lasting oligemic element of the CBF response is detectable to the first SD only [51, 57, 58]. Our present data demonstrate that the recovery of tissue pH from the SD-related acidosis also depends on the rank of an SD event in a sequence. More specifically, pHe as well as pHi returned to a more acidic baseline after the first SD with respect to original baseline (pH 7.14±0.11 vs. 7.29±0.02 and 0.047±0.03 vs. -0.0002±0.02 ΔF/F, respectively) coincident with the oligemic phase of the CBF response (Fig. 14). Tissue pH following each subsequent SD then gradually approximated the baseline prior to the first SD (Fig. 14) in contrast with CBF, which did not recover from oligemia (Fig. 14).

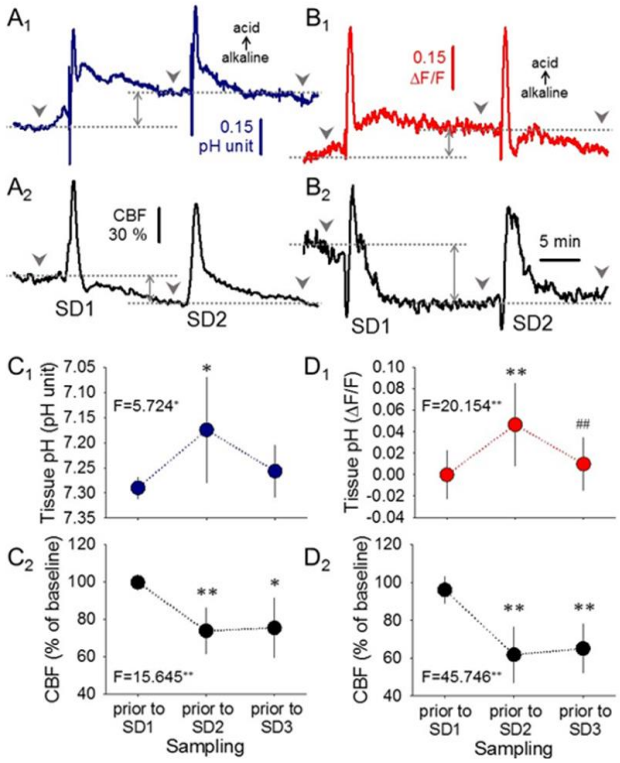

Figure 14. Tissue pH changes with the first spreading depolarization (SD) event differ from subsequent recurrent SDs. A, Representative traces of tissue pH variations (blue) and the associated cerebral blood flow response (CBF) (black) acquired with a pH-sensitive microelectrode and laser Doppler flowmetry from the young intact rat cortex. B, Representative traces of Neutral red fluorescence imaging (red) indicative of tissue pH and the associated CBF response (black) acquired with laser speckle contrast analysis. Note that tissue pH remains acidic after the first SD, concomitant with post-SD oligemia. C & D, Mean values of baseline tissue pH (C1 and D1) and corresponding CBF (C_2 and D_2) taken at the time points indicated by gray arrow heads in panels A and B.

Data are given as mean±stdev. Statistical analysis relied on a repeated measures ANOVA paradigm (F value is given in each plot, levels of significance were determined as $p<0.05$* and $p<0.01$**) followed by pairwise comparisons ($p<0.05$* and $p<0.01$** vs. prior to SD1; $p<0.01$## vs. prior to SD2).

We and others occasionally encounter SD-associated, negative DC shifts, which are smaller in amplitude than 5 mV ("mini" SDs). In order to identify the nature of these SDs and to assess their injurious potential, we examined the kinetics of the related tissue pH and CBF transients. The series of experiments involving pH-sensitive microelectrodes demonstrated that the pHe signature of "mini" SDs was devoid of the initial alkaline shift (Fig. 15A), and the relative amplitude of the dominant acidosis was significantly smaller with respect to normal SDs (0.11±0.04 vs. 0.31±0.13 pH units). The relative amplitude of the SD-coupled hyperemia was also markedly reduced for "mini" SDs (29.6±16.5 vs. 55.3±27.2 %). Correlation analysis between the amplitude of the negative DC shift and dominant acidosis with SD revealed a highly significant positive association (Fig. 15B). Examining the videos obtained with NR imaging and LASCA, it has become clear that "mini" SDs as seen on DC potential traces must designate the rim of aborting SD events (Fig. 15C-D).

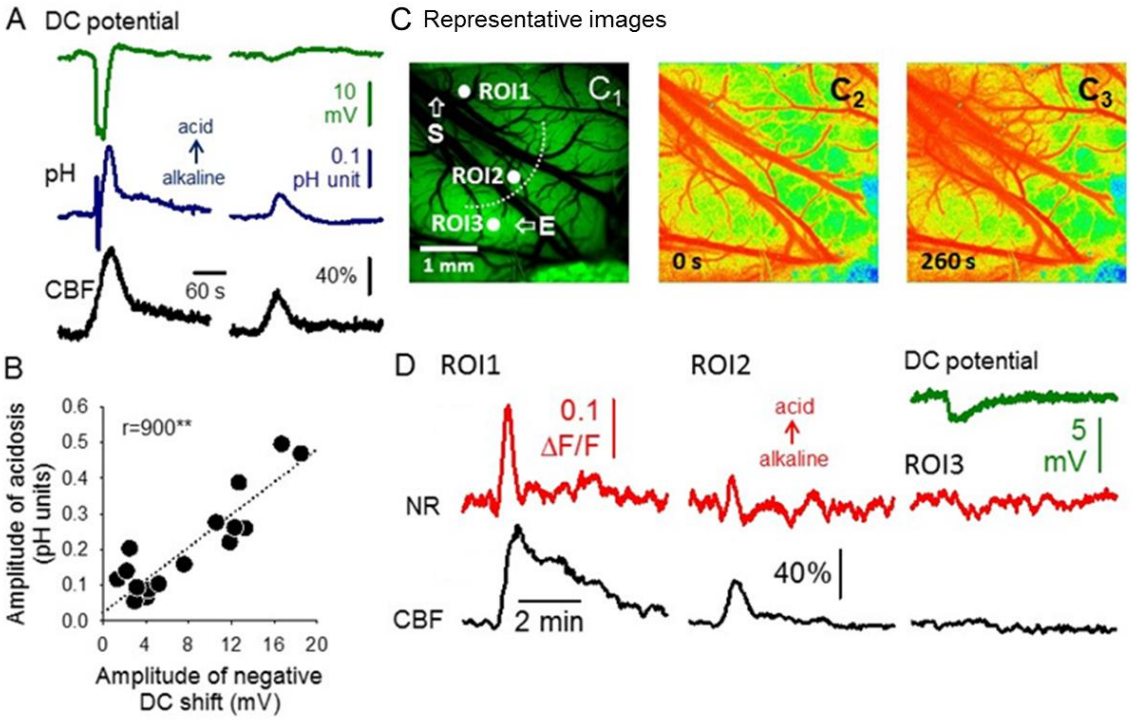

Figure 15. Metabolic correlates and nature of spreading depolarizations (SD) appearing indistinct on the direct current (DC) potential recording. A, Representative traces demonstrate signals corresponding to a conventional DC signature of an SD (left), and a "mini" SD (i.e. amplitude of the negative DC shift less than 5 mV) (right). B, The amplitudes of the SD-related DC shift and acidosis show a direct, linear, positive correlation. C, Images illustrate an SD that was initiated at the stimulating glass capillary (S in C_1), propagated radially, but aborted halfway within the field of view (dotted white line in C_1 indicates the zone where SD came to a halt). C2 and C3 are pseudo-colored perfusion maps based on laser speckle contrast images to demonstrate the cortical area involved in the propagation of the aborting SD (i.e. hyperemia denoted by warm colors spatially extends as far as the SD propagated). C2 and C3 are pseudo-colored perfusion maps based on laser speckle contrast images to demonstrate the cortical area involved in the propagation of the aborting SD (i.e. hyperemia denoted by warm colors spatially extends as far as the SD propagated). D, Traces of Neutral red (NR) fluorescence intensity and cerebral blood flow (CBF) taken at three regions of interest (ROI) shown in C1, and the DC potential signature of a "mini" SD (electrode "E" is shown in C1). ROI3 (indicated in C1) was positioned as near the glass capillary electrode (E in C1) as the pial vascular architecture allowed. Note that the extinguishing SD appears as a "mini" SD at the DC recording site.

3.6. Enhanced tissue acidosis associated with spreading depolarization in the ischemic cortex

Under ischemia, acidosis associated with evoked SDs was substantially augmented (Fig. 16A). This was reflected by the greater relative amplitude with respect to baseline SDs (for young animals, microelectrode: 0.43±0.15 vs. 0.36±0.07 pH units; NR imaging: 0.37±0.18 vs. 0.23±0.10 ΔF/F) (Fig. 14B); the longer duration (for young animals, microelectrode: 93.1±26.3 vs. 40.2±8.1 s; NR imaging: 127.5±64.2 vs. 39.8±13.8 s) (Fig. 16C), the greater magnitude expressed as area under the curve (for young animals, microelectrode: 2415±869 vs. 855±322 pH unit x s; NR imaging: 57.4±50.9 vs. 9.8±5.9 ΔF/F x s), and the slower recovery from acidosis (for young animals, microelectrode: 0.44±0.33 vs. 0.70±0.23 pH

units/s; NR imaging: 0.004±0.002 vs. 0.009±0.005 ΔF/F /s) (Fig. 16D). During reperfusion, the quantitative measures of SD-related acidosis returned to near pre-ischemic values (e.g. for young animals, relative amplitude 0.31±0.09 vs. 0.36±0.07 pH units; duration: 42.0±8.0 vs. 40.2±8.1 s) (Fig. 16B-C).

Aging also had noticeable impact on the pH transients with SDs. Both pH-sensitive microelectrodes and NR imaging indicated consistently that the recovery from acidosis was significantly slower in the old group as compared with the young during baseline (electrophysiology: 0.47±0.24 vs. 0.70±0.26 pH units/s; NR imaging: 0.006±0.003 vs. 0.009±0.005 ΔF/F /s) and ischemia (electrophysiology: 0.23±0.12 vs. 0.44±0.005 pH units/s; NR imaging: 0.002±0.001 vs. 0.004±0.002 ΔF/F /s) (Fig. 16D). Further, NR imaging but not pH-sensitive microelectrodes showed longer-lasting acidosis during ischemia in the old group with respect to the young (197.2±116.7 vs. 127.5±64.2 s). Finally, pH sensitive microelectrodes revealed a smaller amplitude of acidosis in the aged animals, particularly during ischemia (0.31±0.12 vs. 0.43±0.15 pH units) and reperfusion (0.22±0.07 vs. 0.31±0.09 pH units) (Fig. 16B). Nevertheless, the smaller amplitude of acidosis may be, at least partly related to blood pH, since it appeared to coincide with more alkaline blood pH (Fig. 16C) relevant for the electrophysiology series of experiments ($r=-0.584$, $p<0.023$), but not for NR imaging ($r=0.047$, $p<0.432$).

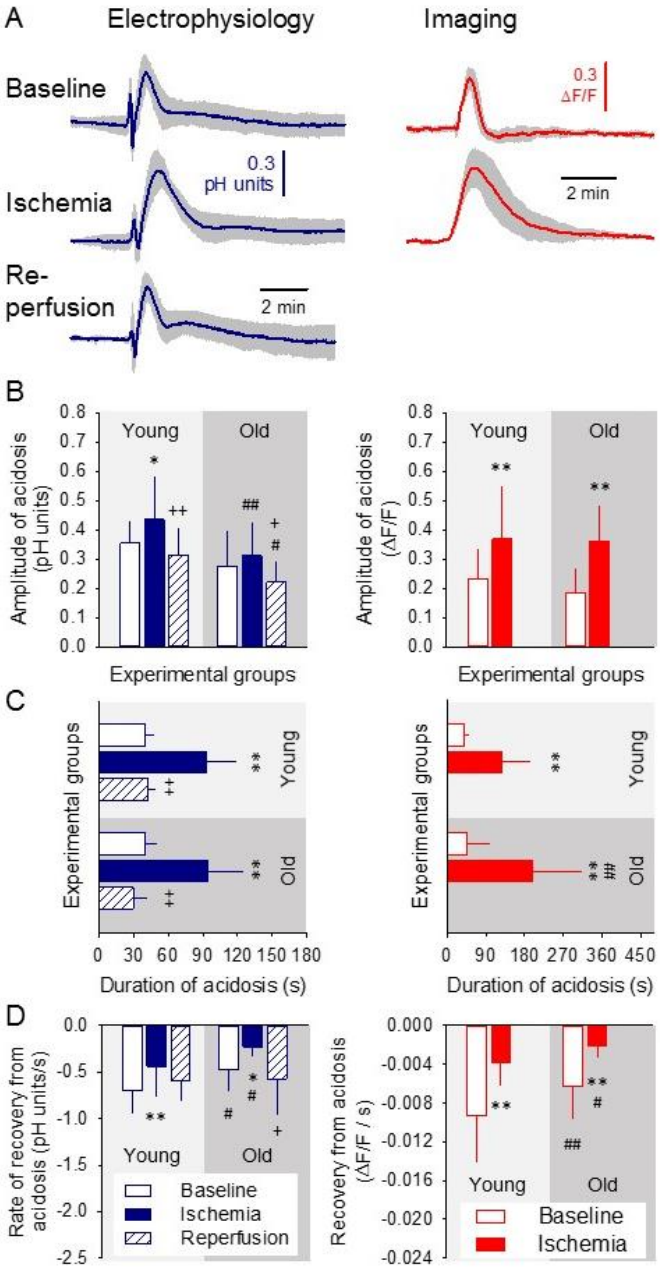

Figure 16. Tissue acidosis with spreading depolarization (SD) is augmented during ischemia, and recovers slower in the aged brain. In each panel, data obtained with pH-sensitive microelectrodes is shown on the left, and data derived from Neutral red fluorescence imaging is shown on the right. A, Tissue pH variations associated with SDs occurring during the three subsequent phases (i.e. baseline, ischemia, reperfusion) of the experiments. Each trace is the average of individual ones taken from separate animals, and are presented as mean±stdev (n=6/8). B, Relative amplitude of acidosis. C, Duration of acidosis at half amplitude. D, Rate of recovery from acidosis (i.e. slope). Data are given as mean±stdev. For the evaluation of statistical significance, a two-way analysis of variance (ANOVA) paradigm considering age and the phase of the experiment as its factors was applied. Level of significance for the ANOVA was defined as $p<0.05$*. Significant differences between groups were determined by a Fisher post hoc test as follows: $p^*<0.05$ and $p^{**}<0.01$, vs. respective Baseline; $p+<0.05$ and $p++<0.01$, vs. respective Ischemia; $p\#<0.05$ and $p\#\#<0.01$, vs. respective Young.

3.7. Cerebral blood flow response to spreading depolarization

The CBF response to evoked SDs was predominantly hyperemic in all experimental groups, except for a few hypoemic transients observed under ischemia. The relative amplitude of hyperemia markedly decreased (for young: 20.8±8.9 vs. 76.3±11.96 %), while its duration more than doubled (for young: 146.4±49.7 vs. 61.4±11.6 s), under ischemia with respect to baseline (Fig. 17). As a consequence, the magnitude of hyperemia expressed as area under the curve was significantly smaller during ischemia (3009±1073 vs. 4428±1436 % x s) (Fig. 17D). The amplitude and magnitude of the hyperemic response during reperfusion was not re-

established to pre-ischemic values, but remained considerably smaller, the magnitude being even similar to that under ischemia (for young: 46.9±25.3 vs. 76.3±119.6 %; 2788±1362 vs. 4428±1436 % x s) (Fig. 17). The impact of age was most of all reflected by the prominent decrease of the magnitude of hyperemia under all three phases of the experiments (i.e. baseline, ischemia and reperfusion) (Fig. 17D).

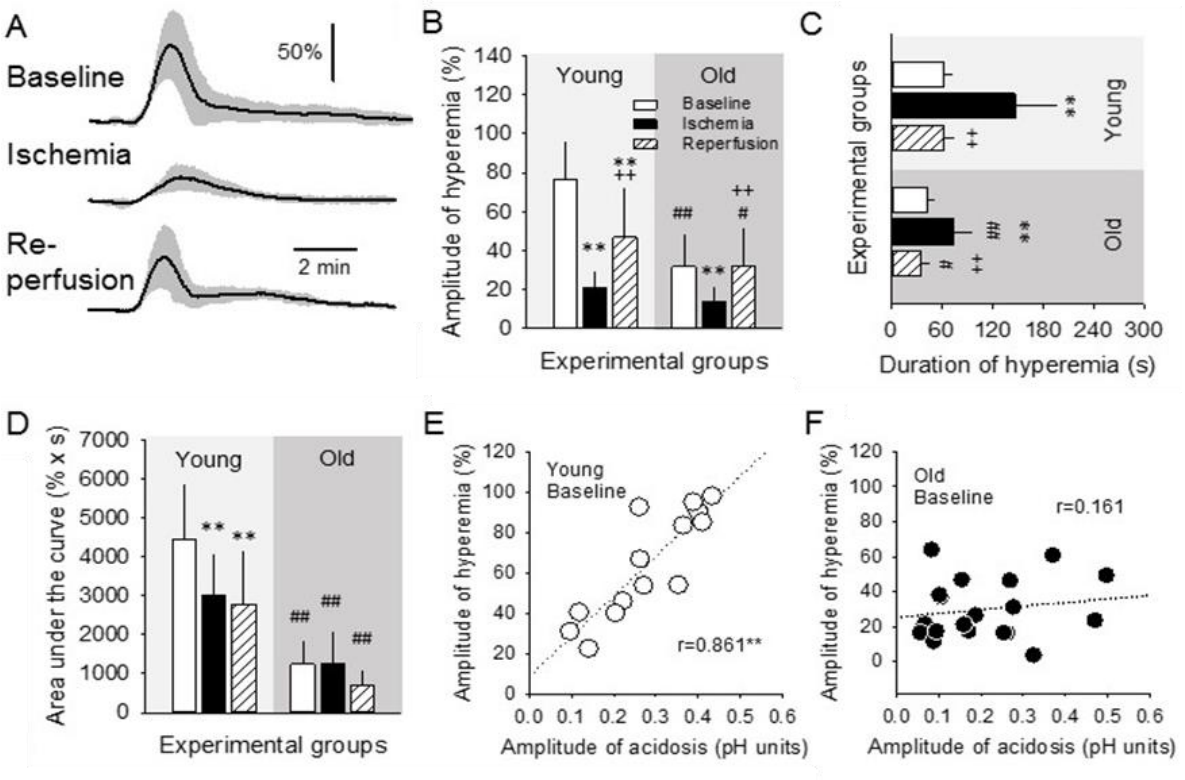

Figure 17. The impact of age and tissue pH on the cerebral blood flow (CBF) response to spreading depolarization (SD). All data were obtained with laser Doppler flowmetry and pH sensitive microelectrodes (the latter applicable for panels E and F). A, CBF variations associated with SDs, occurring in subsequent phases (i.e. baseline, ischemia, reperfusion) of the experiments in young rats. Each trace is the average of individual ones taken from separate experiments, and are presented as mean±stdev (n=6/8). B, Relative amplitude of hyperemia. C, Duration of hyperemia at half amplitude. D, Magnitude of hyperemia expressed as area under the curve. E, The relative amplitude of SD-related tissue acidosis and hyperemia show a direct, linear, positive correlation in the intact cortex of young rats. F, The above correlation is lost in the intact cortex of old animals. Data in the bar charts are given as mean±stdev. For the evaluation of statistical significance, a two-way analysis of variance (ANOVA) paradigm considering age and the phase of the experiment as its factors was applied. Level of significance for the ANOVA was defined as $p<0.05$* and $p<0.01$**. Significant differences between groups were determined by a Fisher post hoc test as follows: p*<0.05 and p**<0.01, vs. respective Baseline; p+<0.05 and p++<0.01, vs. respective Ischemia; p#<0.05 and p##<0.01, vs. respective Young. Correlation in E and F was tested by Pearson one-tailed correlation analysis ($p<0.01$**).

We examined whether the evolution of hyperemia was associated with tissue pH changes and found in the young animals that the higher amplitude of acidosis clearly coincided with the higher amplitude of hyperemia in all three phases of the experiments (baseline: r=0.861, $p<0.0001$; ischemia: r=0.430, $p<0.02$; reperfusion: r=0.534, $p<0.02$), the association being strongest during baseline (Fig. 17E). In contrast, such correlation could not be discovered in

the old animals (e.g. baseline: r=0.162, p<0.254) (Fig. 17F). The duration of hyperemia, on the other hand, appeared to be unrelated to the duration of acidosis in both age groups (e.g. young baseline: r=0.371, p<0.096; old baseline: r=0.193, p<0.215).

3.8. Aggravation of ischemia-induced tissue acidosis by spontaneous spreading depolarization

The evaluation of spontaneous SDs delivered, perhaps, the most revealing findings of the present study. A single spontaneous SD event occurred within 2 min after ischemia induction in a total number of 15 out of 33 experiments. The distribution of these animals with respect to experimental methods and age groups is shown in Figure 18D. Imaging identified that the spontaneous events entered the field of view at the frontal or lateral edges of the cranial window, being generated distant to SDs evoked with KCl application near the medial border of the cranial windows (Fig. 18). Overall, spontaneous SDs were observed more frequently in old animals (12 of 15 cases), but careful analysis of CBF and pH conditions around the time of spontaneous SD evolution suggested that a drop of CBF below 22-23% due to ischemia induction, or ischemia-induced acidosis greater than 0.2 pH units favored SD occurrence (Fig. 18E-F), rather than old age by itself. Also, pHe prior to ischemia induction was significantly more alkaline in cases when spontaneous SD occurred shortly after ischemia onset (electrophysiology: pH 7.28±0.06 and 7.32±0.05 vs. 7.21±0.04, young with spont. SD and old with spont. SD vs. young with no spont. SD).

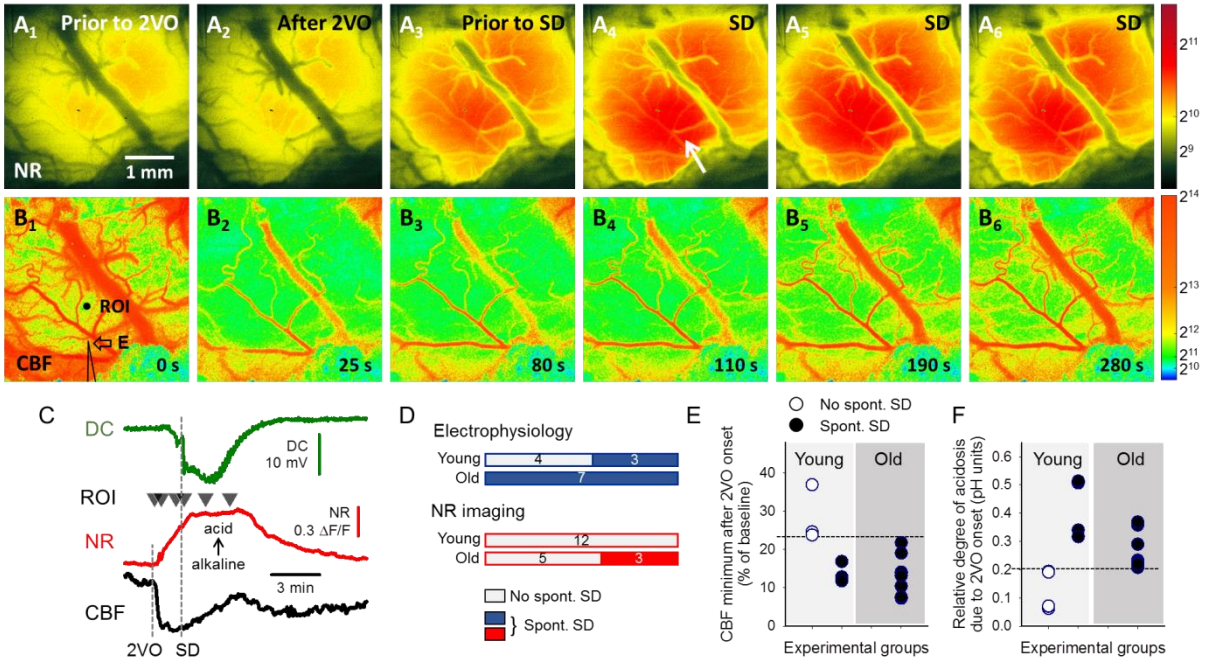

Figure 18. Representative raw image sequences and graphs displaying relative variations illustrate synchronous changes in Neutral Red (NR) fluorescence (A), cerebral blood flow (CBF) (B), and direct current (DC) potential (C), with the propagation of a spontaneous spreading depolarization (SD) wave in the ischemic cerebral cortex of an old rat. Pseudo-colored NR images in Panel A were derived from monochrome images relying on a 16-bit grayscale, while pseudo-colored CBF maps in Panel B display speckle contrast perfusion units. Scale bars to the right represent the used ranges of gray levels. In Panel A4, the entry to the field of view and direction of propagation of a spontaneous SD is shown by a white arrow. In Panel B1, the penetration site of the glass capillary electrode (E) inserted to acquire electrophysiological signals is shown with an arrow, and a region of interest (ROI) indicates the origin of NR and CBF traces shown in Panel C. C, Traces demonstrate the onset of ischemia (2VO) and the evolution of a spontaneous SD as shown by the DC potential signature (green), and the ischemia or SD-related relative changes in NR fluorescence (red) and CBF (black). Small black triangles pointing down over the NR traces designate the origin of the representative images shown in Panels A-B. D-F, Conditions that favor the spontaneous occurrence of SD shortly after ischemia onset are presented. D, Ratio of experiments devoid of spontaneous SD (white) and in which spontaneous SD occurred (colored). Each horizontal box represents the total number of experiments taken as 100%, number of rats is given in the middle of bars. E, Drop of cerebral blood flow (CBF) after ischemia induction, depicted for each experiment involving pH-sensitive microelectrodes. F, The relative amplitude of acidosis induced by ischemia alone, measured directly prior to the detection of SD, for each experiment involving pH-sensitive microelectrodes. Horizontal lines drawn in E and F indicate a theoretical level of threshold for the evolution of spontaneous SD.

The consequences of spontaneous SDs were grave. The SD-related acidosis was superimposed on ischemia-induced acidosis (Fig. 19A) thereby transiently decreasing pHe from the ischemia-related value of 6.93±0.09 to as low as pH 6.48±0.16 in the young group, and from the ischemia-caused pH 7.06±0.10 to 6.76±0.20 in the old animals (Fig. 19B). NR imaging in the old group showed that the occurrence of spontaneous SD more than doubled NR fluorescence intensity with respect to that achieved by ischemia alone (Fig. 19C). Tissue pH in young animals measured over 10 min after spontaneous SD settled to a value more acidic than that produced by ischemia alone at a corresponding point of time (pH 7.09±0.09

vs. 7.29±0.16), which was further worsened by age, as pHe after spontaneous SD was maintained at an average of pH 6.94±0.08 in the old animals (Fig. 19D-E).

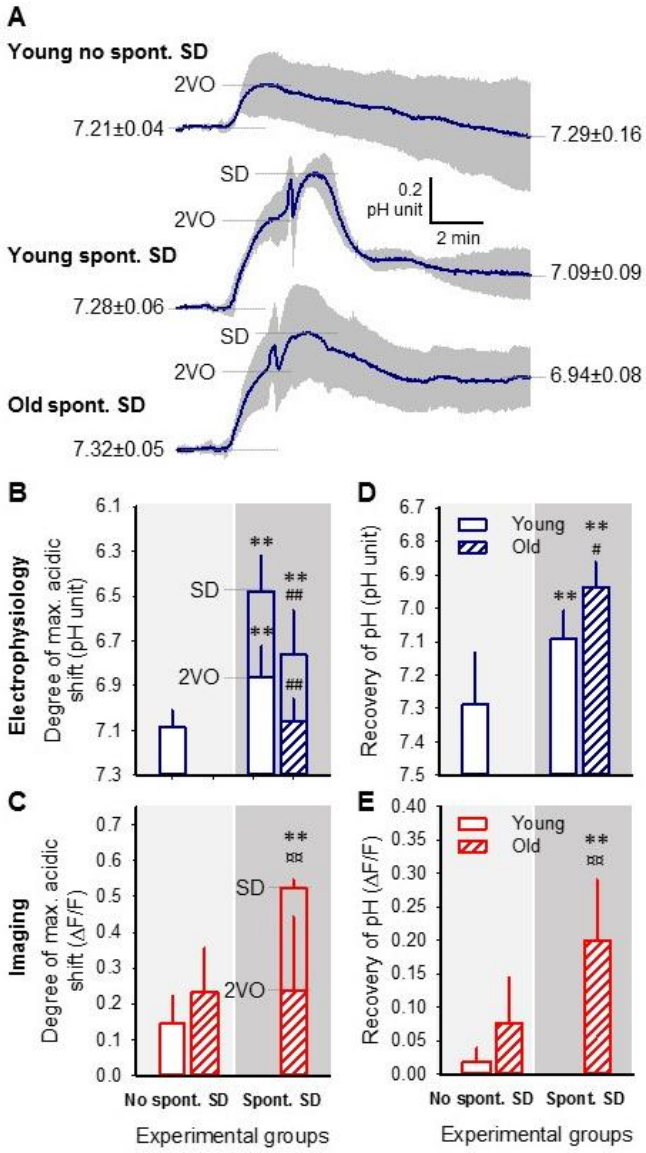

Figure 19. Analysis of pH variations induced by ischemia and spontaneous spreading depolarization (SD). A, Tissue pH variation due to ischemia induction (2VO) and spontaneous SD are superimposed. Each trace is the average of individual ones taken from separate animals, and are presented as mean±stdev (n=6/8). In Panels B, C, D and E, the upper bar charts represent data obtained with pH-sensitive microelectrodes (blue), and the lower bar charts demonstrate data derived from Neutral red (NR) fluorescence imaging (red). Light shaded background of the bar charts (left) labels experiments devoid of spontaneous SD, and dark shaded background in the bar charts (right) stands for experiments in which spontaneous SD occurred. B-C, Amplitude of acidosis. D-E, Tissue pH assessed 12 min after SD occurrence (i.e. tissue pH recovery). For the evaluation of statistical significance, a two-way analysis of variance (ANOVA) paradigm considering age and the occurrence of spontaneous SD as its factors was applied. Level of significance for the ANOVA was defined as $p<0.05$* and $p<0.01$**. Significant differences between groups were determined by a Fisher post hoc test as follows: p*<0.05 and p**<0.01, vs. respective Young; p#<0.05 and p##<0.01, vs. respective with no spontaneous SD.

4. Discussion

4.1. Experimental Project I.

4.1.1. Advantages and limitations of the experimental approach

Experimental studies that set ischemic SDs as their target of investigation predominantly rely on focal ischemia models, in which recurrent SDs occur spontaneously; yet, the systematic analysis of spontaneous SDs remains challenging. Even widely accepted ischemia models,

such as middle cerebral artery occlusion are known to produce quite some variation in ischemia severity [59] - probably because of the anatomic variation in middle cerebral artery branching patterns [60, 61] - which, in turn, will cause variations in the site of SD elicitation, direction of SD propagation, SD type (i.e., short transient or prolonged), and SD pattern (i.e., single events or clusters). A further, inherent limitation of this approach is that nonischemic time control cannot be implemented due to the unpredictable occurrence of spontaneous SDs. For these reasons, we imposed 2VO, which produces an immediate, reproducible drop in CBF without the successive occurrence of multiple spontaneous SDs in adult Sprague-Dawley rats [62]. Additional benefits of the 2VO model allowed:

1) planned, controlled SD elicitation during ischemia by the topical application of KCl
2) the design of nonischemic time control experiments
3) evaluation of ischemic SDs with respect to SDs in the intact or reperfused cortex

Despite these major advantages of the model, some shortcomings have emerged during the progression of Experimental Project I. First, the elicitation of SDs by continuous exposure of the brain surface to KCl [63] produced SDs at a rather high and random frequency. In order to achieve controlled SD elicitation (i.e. a single event in response to triggering), we refined our approach in Experimental Project II as follows. In the open cranial window preparations, a 1M KCl soaked cotton ball was placed and soon removed from the brain surface immediately after SD detection. The subsequent, distinct event was triggered 15 min later. In the closed cranial window preparation, 1 µl 1M KCl was ejected on the exposed brain surface, and then rinsed by continuous irrigation with aCSF. This was repeated at 15 min intervals to achieve the recurrent elicitation of single SDs.

Second, the unexpected condition that 1M KCl will not generate SDs in old rats, together with the necessity to produce SDs to assess age-related features of SD evolution prompted us to use higher concentration or larger volume of KCl for SD induction in old rats. This led us to conclude that the SD threshold must be significantly higher in the aged brain (consistent with previous observation on brain slices) [64] but did not allow the precise quantification of SD threshold.

Finally, the study was conducted with the use of 2 distinct anesthetic agents and mixed strains of rats due to uncontrollable external conditions. Still, the acquired data are highly consistent with our previous findings obtained with the use of halothane anesthetized Wistar rats [46]. Furthermore, we carefully considered any potential impact of the type of anesthesia on all the read-outs presented, by including the type of anesthesia as a factor into the statistical analysis.

This approach excluded the possibility that halothane and isoflurane affected MABP, the DC potential signature of SD or CBF differently.

4.1.2. The recovery of resting membrane potential after depolarization is delayed during ischemia and in old age

In the present study, the longer duration of SD in the ischemic brain is attributed to the collective, lower rate of depolarization and repolarization, rather than the prolongation of complete depolarization itself [65]. During the depolarization phase of SD, there is an intense efflux of K^+ to the extracellular space, parallel with considerable influx of Na^+ [17, 66]. In ischemia, the concentration gradient between the intracellular and extracellular compartments becomes lower than in physiological brain tissue (i.e., $[Na^+]_e$, decreases from 140 to 80 mM, $[K^+]_e$ increases from 5 to 20-60 mM), with parallel but opposite changes in intracellular ion composition [67]. This results in a considerably reduced (but still substantial) transmembrane ionic concentration gradient during SD in the ischemic brain tissue [17]. Therefore, the driving force for K^+ efflux and Na^+ influx that take place during the depolarization phase of SD may decrease, which is thought to be reflected in the lower rate of depolarization as measured here.

The optimal function of Na^+/K^+-adenosine triphosphatase (ATPase) is essential for the restoration of membrane potential following SD. During ischemia, oxidative substrate supply declines, and tissue ATP availability decreases, which lead to the reduction of Na^+/K^+-ATPase activity [30], thereby potentially delaying the restoration of transmembrane potential.

Old-age aggravated the ischemia-related prolongation of SD duration: 1 of the 6 animals in the old 2VO group displayed terminal depolarization, and the duration of transient first SDs was significantly longer as compared with the young 2VO group. These results stand in agreement with our previous observation made in a focal forebrain ischemia model that the cortical surface involved in prolonged SDs was significantly larger in old as compared with young rats [46]. These data together indicate that the aged ischemic brain has scarcer resources to recover from an SD event, which reflects the increased vulnerability of the aged brain to ischemia- and/or SD-related injury.

Finally, the DC potential signature of SDs revealed that the amplitude of hyperpolarization in old rats was approximately half of their young counterparts. Hyperpolarization after SD appears to be a transient overshoot of either $[Na^+]_e$ due to the increased activity of Na^+/K^+ ATPase, or $[Cl^-]_e$ [66]. Aging may have an impact on either of these ion fluxes; yet it remains uncertain which exact mechanism(s) must be responsible for the age-related reduction in the amplitude of hyperpolarization seen in our study.

4.1.3. The hyperemic response to spreading depolarization diminishes during ischemia and becomes inverted in the aged ischemic brain

As presented in the Introduction, the SD-coupled CBF response in the physiologically intact rat cortex consists of at least 4 distinct elements: an initial transient vasoconstriction, a marked hyperemia, a slight late hyperemia and a long-lasting oligemic phase [15]. Ischemia shifts this balance toward the domination of the initial vasoconstrictive (hypoemic) element of the pattern, possibly as a function of decreasing perfusion pressure [28, 65]. Matching this concept, we have identified 6 types of CBF kinetics ranging from dominating hyperemia to prolonged cortical spreading ischemia with intermediate forms. The types observed during ischemia have, coincidentally, a perfect match with those described earlier in the ischemic cortex of stroke patients [29].

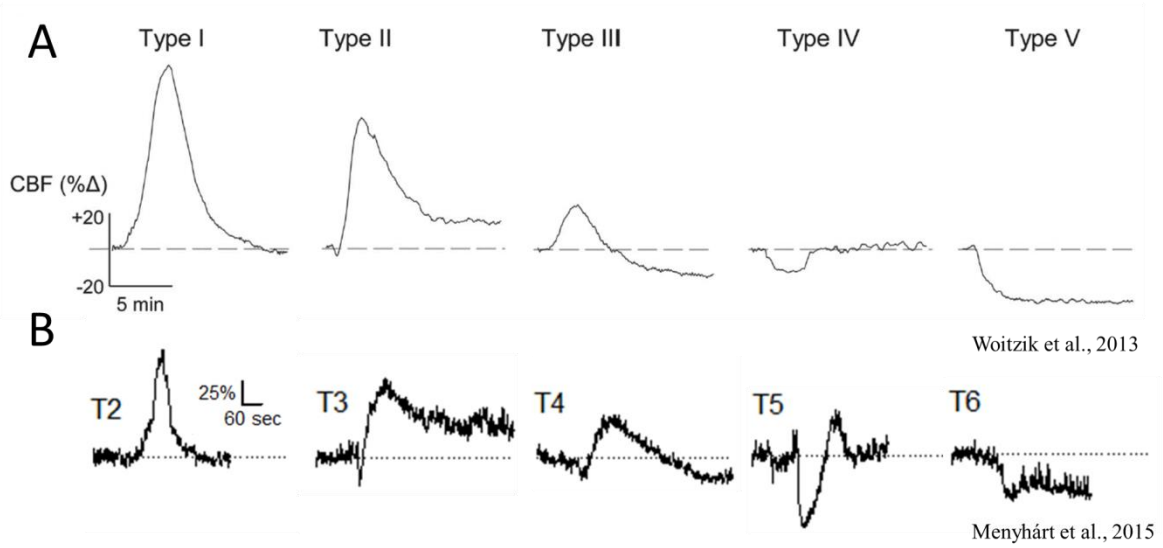

Figure 20. Comparison of the distinct types of cerebral blood flow (CBF) response to spreading depolarization (SD) detected in the cerebral cortex of ischemic stroke patients (A) and in our present experimental study (B).

Our main observations of the SD-related CBF response are as follows: (1) the SD-coupled CBF response types, in which the hypoemic component is augmented at the expense of the hyperemic component, occur more frequently in the aged brain, (2) the combination of ischemia and old age predisposes the cortex for the evolution of spreading ischemia (inverse neurovascular coupling), and (3) the ischemia-related perfusion deficit progressively deepens in the old brain as opposed to the young. During physiological aging, unfavorable changes occur in the brain's microcirculation, including increased vascular wall stiffness [38], decreased vascular density [39], impaired microvascular reactivity [40], and weakened remodeling potential [39]. The additive outcome is lower basal CBF, but more importantly, reduced, suboptimal local

CBF elevation in response to neural activity, which is suggested to contribute to the shift to less obvious hyperemic and more prominent hypoemic elements in the SD-associated CBF response.

The high incidence of inverse coupling in the old ischemic rats (also seen in our previous study concerning focal cerebral ischemia, [46]) is proposed to be determined by the combination of vasoconstrictive high $[K^+]_e$ and the restricted availability of the vasodilator nitric oxide (NO) [68]. Ischemia itself imposes considerable extracellular K^+ accumulation above the dilation and/or constriction threshold (20 mM) [66], and NO is quickly eliminated by its reaction with superoxide yielding peroxynitrite [69]. Limited NO availability due to increased free radical production causes dysfunctional NO-based vasodilation during physiological aging, as well [70, 71]. Ischemia superimposed on aging, therefore, is thought to potentiate the impairment of NO-based vasoregulation in the face of high $[K^+]_e$, which may lead to a higher incidence of inverse neurovascular coupling in the aged ischemic brain. In turn, the resultant spreading ischemia is suggested to deepen the perfusion deficit imposed by ischemia.

4.1.4. Perfusion deficit during ischemia deepens progressively in the aged but not in the young brain

CBF sharply drops after ischemia onset, but compensation through collaterals or vascular remodeling may contribute to slow partial recovery of perfusion [46, 72]. Our data indicate that in the ischemia model used, perfusion stabilized and persisted at around 40% till the end of the ischemic period in young rats, but dropped below 20% in old rats, which falls below the CBF threshold of electrical failure of the nervous tissue [3]. Although age related cerebrovascular rarefaction may be held responsible for the poor flow compensation in aged rats [39], we believe that the ischemia-induced perfusion deficit in our study was aggravated by the high incidence of inverse neurovascular coupling with SD in old animals. Thus, SDs associated with spreading ischemia likely impair the recovery of CBF, thereby worsening ischemia outcome.

4.2. Experimental Project II.

4.2.1. Tissue pH imaging with Neutral Red

Even though in vivo, live imaging of brain pHi with NR had been achieved previously [48, 49, 73], our approach presented here reaches further and is unique in that NR fluorescence indicative of pHi was supported by and correlated with the conventional pHe signal acquired with pH-sensitive microelectrodes.

Intracellular acidosis with SD, as indicated by NR fluorescence must represent a sum of neuronal and astrocytic pH transients, assuming that both cell types incorporate the dye, and accepting that contribution of NR circulating in blood plasma is negligible [47]. During SD in the intact cortex, astrocytes display a considerable alkaline pHi shift of 0.28 pH units [74]. Much less is known about distinct pHi variations of neurons during SD, but a recent study has revealed that neurons undergo intracellular acidosis with SD onset, as demonstrated by selectively loading these cells in neocortical brain slices with the pH-sensitive fluorescent dye BCECF [75]. Taken together, the SD-associated pHi signal of NR in the intact cortex is presumed to be dominated by neuronal acidosis versus astrocytic alkalosis.

We have found a good correlation between intra- and extracellular acidosis during SD (Fig. 12A). This stands in agreement with the finding that newly produced lactate is readily released from neurons and from astrocytes to the extracellular space by lactate-proton cotransport [76], and with the suggestion that pHi and pHe decrease parallel at increasing lactate concentration in the ischemic tissue [77].

Three elements of the pHe signature of SD did not appear on the pHi traces. The initial, brief acidic shift was most certainly an artefact created when the reference was subtracted from the raw pH signal, because the tips of the two electrodes could not possibly be located at an identical spot [23]. The subsequent alkaline shift was previously attributed to the efflux of $HCO3^-$ from cellular compartments to the interstitium [23, 78]. Finally, the more gradual recovery of pHe with respect to pHi probably followed the rate of lactate recycling or extrusion to the blood stream [22].

4.2.2. Spreading depolarization during ischemia and associated tissue pH variations

Brain pH measurement has delivered three novel observations, with neurological consequences that are anticipated to be significant: (i) The SD-related acidosis is remarkably enlarged in the ischemic as compared with the intact cortex; (ii) SD-related acidosis evolving in the ischemic cortex is additive to ischemia-induced acidosis.; (iii) In the aging brain, the recovery from SD-related acidosis is hampered, and tissue pH subsequent to SD remains more acidic with respect to the young cortex.

The intensification of SD-related acidosis under ischemia has been characterized here by the higher relative amplitude and longer duration of the acidic pH transients (Fig. 16). Previous observations suggest, that tissue acidosis associated with SD in the intact cortex must depend on the concentration of lactate produced, because pHe was shown to decrease synchronously with the elevation of lactate [22, 23]. In support of the lactate-dependence of tissue acidosis, a

linear correlation was established between increasing lactate levels and decreasing tissue pH in the ischemic brain [77, 79]. Based on the evidence listed here, we propose that the greater amplitude of SD-related acidosis in ischemic with respect to the intact cortex must be caused by the increased accumulation of lactate. Because lactate is generally the product of anaerobic metabolism, we speculate that lactate concentration, and thus the relative peak of acidosis associated with SD depends on whether the tissue can initially utilize aerobic metabolic pathways in response to SD [20, 80], or relies largely on anaerobic metabolism setting already in before SD generation, because of ischemia [81]. The longer duration of SD-related acidosis and the underlying lactate production during ischemia, on the other hand, possibly correlate well with delayed repolarization [30, 82], thus with the continuing demand for energy.

In addition to the finding that acidosis with SD is markedly enhanced in the ischemic cortex, we have also demonstrated here that the SD-related acidosis is additive to ischemia-induced acidosis, especially with spontaneous SDs (Fig. 19). Our global forebrain ischemia model created conditions similar to the ischemic penumbra, in that CBF dropped below 40 %, and remained between 20-40 % until reperfusion was initiated [3, 83]. Prior to the detection of the propagating spontaneous SD, pHe ranged between pH 6.9-7.0 in the cortex, similar to pHi that was calculated for the penumbra region after middle cerebral artery occlusion (MCAO) [84]. Acidosis associated with SD here shifted pHe to as low as pH 6.48 in average, more typical of the ischemic core of focal insults. For comparison, focal ischemia upon onset produced tissue pH of 6.64 in the rabbit cortex [36], and pH 6.53 at the peri-infarct rim after MCAO in rats [83]. Taken together, we propose that SDs that propagate over the ischemic penumbra transiently increase local acid load to cytotoxic levels typical of the ischemic core, which may be a potent pathophysiological mechanisms to cause neurodegeneration. Furthermore, not only the amplitude but also the duration of acidosis was shown to jeopardize tissue integrity. As such, the prolongation of acid exposure was concluded to reduce the threshold of acid-induced cell death [34]. Taken that SDs occur in a recurrent fashion in ischemic zones [11, 12], and that tissue pH remains acidic for at least 10 min after an SD event propagating under penumbra-like conditions (Fig. 19), SDs are suggested to prolong tissue acidosis, thereby also increasing the risk of neuronal injury.

The spontaneous generation of SD was more frequently encountered in the old animals. Previously, we reported that spontaneous SDs emerged less frequently in the old brain with respect to the young in a rat model of focal ischemia, probably because longer-lasting depolarizations prevented the occurrence of subsequent SDs [46]. Here we show that SD occurs

spontaneously when the perfusion deficit shortly after ischemia onset is severe (CBF drop to between 7-23 %, albeit measured distant to the exact site of SD generation), which was encountered more frequently in old animals (Fig. 18E). These results corroborate the opinion that the aged nervous tissue is more susceptible to hypoxic or ischemic injury [41], most certainly because its inherent sensitivity [85] is challenged further by a deeper cerebral perfusion deficit after cerebral vessel obstruction. In turn, the supply-demand mismatch for energy substrates becomes aggravated, which makes the occurrence of SD more likely [25]. This initiates a vicious cycle more prominent in the aged brain, as SD deepens the metabolic crisis even further, and ultimately worsens tissue outcome [26, 30]. In summary, our results reveal that in the aged brain the occurrence of SD is facilitated because the perfusion deficit is graver. Moreover, we propose, that the aging brain may be at higher risk for acid-induced neurodegeneration, because tissue pH after the passage of an SD remains significantly more acidic with respect to the young brain (Fig. 19D-E). Finally, the age-related metabolic pattern of SD evolution shown here is suggested to substantiate the accelerated conversion of ischemic penumbra into infarction with age, as was described earlier in patients [43].

4.2.3. Cerebral blood flow response to spreading depolarization, and its association with tissue pH

The impairment of the CBF response to SD during ischemia (Fig. 17) clearly confirms our previous reports [57, 82]. However, it has not been demonstrated that the CBF response to SD remains insufficient during reperfusion, as well. Since our CBF measurements focused on the microvascular bed, it is plausible that capillary reflow impaired by oxidative-nitrative stress-related pericyte constriction [86, 87] contributed to the insufficiency of the CBF response during reperfusion.

We found a strong positive correlation between the peak of acidosis and of hyperemia to SD in the young cerebral cortex (Fig. 17E). At close inspection, the imaging experiments revealed that the peak of acidosis preceded slightly the peak of hyperemia to SD (Fig. 11). If these observations represent more than a coincidence, it would appear that the coupling during SD must have a metabovascular component, even though the prevalence of neurovascular over metabolic coupling with SD has been promoted [15]. Our data further indicate, that if such a coupling exists, it is severely impaired in the aged brain (Fig. 17F).

5. Main observations and conclusions

The SD-coupled CBF response types, in which the hypoemic component is augmented at the expense of the hyperemic component, occur more frequently in the **aged** brain and the combination of ischemia and **old age** predisposes the cortex for the evolution of spreading ischemia (inverse neurovascular coupling)

The relevance of our **aged** rat models is substantiated by the reported statistics about the incidence of ischemic stroke [41]. The fact, that our observed SD-related CBF response types perfectly matched with those described earlier in the ischemic cortex of stroke patients [29] intensifies the translational potential of this work. However, the next steps should focus on the understanding of the background mechanisms underlying spreading ischemia. Therefore, further investigations on **aged** rats are required for better understand the exact mediators of cortical spreading ischemia.

SD-related progression of neuronal injury in the ischemic penumbra was previously attributed to hypoperfusion in response to SD, known as inverse hemodynamic response or spreading ischemia [30]. Such insufficiency of the CBF response to SD delays repolarization and causes excitotoxic damage, ultimately leading to cell death [26]. However, only a fraction of SDs propagating across the ischemic penumbra are coupled with spreading ischemia [57 82] and it has remained uncertain what mechanism might mediate neurodegeneration in case the hemodynamic response to SD is hyperemic. Altered brain metabolism due to vascular occlusion features the utilization of acid based metabolites, such as CO_2 and lactate which are vasoactive molecules and could regulate the cerebrovascular tone [88]. Here we present, that tissue pH drops remarkably with each SD propagating across the ischemic cortex, to which hyperemic CBF response is coupled. We propose that this acidic shift in tissue pH with recurrent SDs is additive and cytotoxic, consistent with the view that marked acid accumulation correlates with the extent of brain injury, and that tissue acidosis is a damaging component of cerebral ischemia [35].

The long cumulative duration of ECoG depression associated with recurrent SDs has been suggested as an early marker of delayed ischemic brain damage [13]. Based on our present results, tissue acidosis may be a sensitive indicator of potential tissue injury as well, and may be indirectly monitored in intensive care units by the use of lactate biosensors [89]. We propose that the SD-associated, prominent, transient acidosis superimposed on ischemia-induced acidosis worsens tissue survival, thereby rendering SDs a causative, malignant event in

cerebral ischemia. In contrast, the less pronounced pH changes with SDs in the non-ischemic cortex are suggested not to be directly harmful. Instead, SD-associated mild acidosis appears to be neuroprotective by suppressing the excitability of neurons and delaying the occurrence of subsequent SDs [90].

6. Summary

Background: Aging emerges as a major independent risk factor for the incidence and prevalence of ischemic stroke and predicts poor patient outcomes [41, 42]. In our aging population, much of the primary injury in the acute phase of ischemic stroke may prove irreversible, yet the management of secondary pathophysiological processes is of fundamental importance to improve the prospect of successful recovery. Spontaneously occurring recurrent spreading depolarizations (SDs) were recognized as contributors of the expansion of cerebral tissue damage following subarachnoid hemorrhage, stroke or traumatic brain injury [26].

Hypothesis: Since the aged brain is more susceptible to ischemia- and SD-related injury [45, 46], we hypothesized, that (1) the evolution of SDs and the related hemodynamic responses could be altered by aging and (2) the SD associated metabolic changes, such as tissue acidosis should also be graver in the aged ischemic brain.

Aims: We set out to determine; (1) the impact of age on the evolution of SD and the kinetics of the associated changes in local CBF in the intact and ischemic rat brain, (2) the impact of age on the SD related tissue pH changes in the intact and ischemic rat brain, and (3) the association between the SD-related pH transients and SD-related CBF responses.

Methods: Open or closed cranial windows were mounted on the parietal bone of halothane or isoflurane-anesthetized young (2-months-, n=33) and old (18-20-month-old, n=18, and 2-year-old, n= 26) Sprague Dawley or Wistar rats. Mean arterial blood pressure and arterial blood gases were monitored via a femoral artery catheter. Transient incomplete global forebrain ischemia was achieved by the bilateral occlusion of the common carotid arteries (2VO). SDs were elicited by the topical application of KCl. The evolution of SDs and –the associated local CBF changes were acquired by the measurement of DC potential and laser-Doppler flowmetry. SD-related variations in extracellular pH were acquired with pH-sensitive microelectrodes inserted into the cortex. SD-coupled intracellular pH- and perfusion changes

were monitored relying on the fluorescence intensity of a pH indicator dye (Neutral Red), and laser speckle contrast analysis, respectively.

Results: Ischemia elongated the duration of the SD-related negative DC shift (66.2±22.8 vs. 21.4±4.1 s, Young 2VO vs. Young control), which was augmented further by age as seen in the Old 2VO group (95.8±46.2 s). Six types of SD-coupled CBF responses were identified, ranging from dominating hyperemia to prolonged cortical spreading ischemia with intermediate forms. Spreading ischemia evolved only in the aged ischemic group (4 of the 6 animals). Quantitative analysis of the duration of early hypoperfusion indicated that this first element of the CBF response to SD was elongated during ischemia (36.8 ± 17.5 vs. 7.9 ± 6.8 sec, Young 2VO vs. Young control) and became drastically longer in the Old 2VO group (1344 ± 1047 sec), due to the prevalence of spreading ischemia.

Acid accumulation with SDs propagating across the ischemic cortex was considerably increased with respect to the intact and reperfused condition (e.g. relative amplitude of acidosis: pH 0.43±0.15 vs. 0.36±0.07 vs. 0.31±0.09, ischemia vs. intact vs. reperfused). Tissue acidosis with SD was additive to ischemia-induced acidosis thereby raising acid load to potentially cytotoxic levels (level of acidosis: pH 6.48±0.16 vs. 6.93±0.09, with SD under ischemia vs. ischemia alone prior to SD onset). In addition, tissue pH remained acidic for at least 10 min after the passage of an SD (pH 7.09±0.09 vs. 7.29±0.16, 12 min after SD vs. time control ischemia without SD), which was further deepened in the aged brain (pH 6.94±0.08 vs. 7.09±0.09, old vs. young).

Discussion: While ischemia clearly compromised the kinetics of SDs and the associated CBF response, age exerted an additional shift to more injurious CBF response types including spreading ischemia. We propose that structural and functional alteration of the cerebro-microvascular system with aging serves as a potential basis for compromised vascular reactivity. The prospect of successful recovery after stroke strongly depends on the metabolic statement of the affected tissue. Marked tissue acidosis correlates with the extent of brain injury, and has been traditionally considered as a damaging component of cerebral ischemia. In conclusion, SDs are suggested to extend ischemic lesions by increasing acid accumulation in the ischemic penumbra to toxic levels characteristic of the ischemic core. Repeated SDs typically evolving in the ischemic cortex are expected to maintain low pH, which decreases the threshold of acid-induced cell death. Finally, the aged brain may be at higher risk for SD-related injury, because the recovery of tissue pH after SD is hampered.

7. References

1. Go AS, Mozaffarian D, Roger VL, et al. Executive summary: heart disease and stroke statistics--2014 update: a report from the American Heart Association. *Circulation* 2014; **129**(3): 399-410.
2. Seshadri S, Wolf PA. Lifetime risk of stroke and dementia: current concepts, and estimates from the Framingham Study. *The Lancet Neurology* 2007; **6**(12): 1106-14.
3. Astrup J, Symon L, Branston NM, Lassen NA. Cortical evoked potential and extracellular K+ and H+ at critical levels of brain ischemia. *Stroke; a journal of cerebral circulation* 1977; **8**(1): 51-7.
4. Fisher M. The ischemic penumbra: identification, evolution and treatment concepts. *Cerebrovascular diseases* 2004; **17 Suppl 1**: 1-6.
5. Hartings JA, Rolli ML, Lu XC, Tortella FC. Delayed secondary phase of peri-infarct depolarizations after focal cerebral ischemia: relation to infarct growth and neuroprotection. *The Journal of neuroscience : the official journal of the Society for Neuroscience* 2003; **23**(37): 11602-10.
6. Astrup J, Siesjo BK, Symon L. Thresholds in cerebral ischemia - the ischemic penumbra. *Stroke; a journal of cerebral circulation* 1981; **12**(6): 723-5.
7. Ramos-Cabrer P, Campos F, Sobrino T, Castillo J. Targeting the ischemic penumbra. *Stroke; a journal of cerebral circulation* 2011; **42**(1 Suppl): S7-11.
8. Dohmen C, Sakowitz OW, Fabricius M, et al. Spreading depolarizations occur in human ischemic stroke with high incidence. *Annals of neurology* 2008; **63**(6): 720-8.
9. Dreier JP, Woitzik J, Fabricius M, et al. Delayed ischaemic neurological deficits after subarachnoid haemorrhage are associated with clusters of spreading depolarizations. *Brain : a journal of neurology* 2006; **129**(Pt 12): 3224-37.
10. Hartings JA, Strong AJ, Fabricius M, et al. Spreading depolarizations and late secondary insults after traumatic brain injury. *Journal of neurotrauma* 2009; **26**(11): 1857-66.
11. Hossmann KA. Periinfarct depolarizations. *Cerebrovascular and brain metabolism reviews* 1996; **8**(3): 195-208.
12. Nedergaard M. Spreading depression as a contributor to ischemic brain damage. *Advances in neurology* 1996; **71**: 75-83; discussion -4.
13. Dreier JP, Fabricius M, Ayata C, et al. Recording, analysis, and interpretation of spreading depolarizations in neurointensive care: Review and recommendations of the COSBID research group. *Journal of cerebral blood flow and metabolism : official journal of the International Society of Cerebral Blood Flow and Metabolism* 2016.
14. Sakowitz OW, Kiening KL, Krajewski KL, et al. Preliminary evidence that ketamine inhibits spreading depolarizations in acute human brain injury. *Stroke; a journal of cerebral circulation* 2009; **40**(8): e519-22.
15. Ayata C, Lauritzen M. Spreading Depression, Spreading Depolarizations, and the Cerebral Vasculature. *Physiological reviews* 2015; **95**(3): 953-93.
16. Pietrobon D, Moskowitz MA. Chaos and commotion in the wake of cortical spreading depression and spreading depolarizations. *Nature reviews Neuroscience* 2014; **15**(6): 379-93.
17. Somjen GG. Mechanisms of spreading depression and hypoxic spreading depression-like depolarization. *Physiological reviews* 2001; **81**(3): 1065-96.
18. Krivanek J. Some metabolic changes accompanying Leao's spreading cortical depression in the rat. *Journal of neurochemistry* 1961; **6**: 183-9.
19. Mies G, Paschen W. Regional changes of blood flow, glucose, and ATP content determined on brain sections during a single passage of spreading depression in rat brain cortex. *Experimental neurology* 1984; **84**(2): 249-58.
20. Mayevsky A, Weiss HR. Cerebral blood flow and oxygen consumption in cortical spreading depression. *Journal of cerebral blood flow and metabolism : official journal of the International Society of Cerebral Blood Flow and Metabolism* 1991; **11**(5): 829-36.
21. Takano T, Tian GF, Peng W, et al. Cortical spreading depression causes and coincides with tissue hypoxia. *Nature neuroscience* 2007; **10**(6): 754-62.

22. Scheller D, Kolb J, Tegtmeier F. Lactate and pH change in close correlation in the extracellular space of the rat brain during cortical spreading depression. *Neuroscience letters* 1992; **135**(1): 83-6.
23. Mutch WA, Hansen AJ. Extracellular pH changes during spreading depression and cerebral ischemia: mechanisms of brain pH regulation. *Journal of cerebral blood flow and metabolism : official journal of the International Society of Cerebral Blood Flow and Metabolism* 1984; **4**(1): 17-27.
24. Nedergaard M, Hansen AJ. Spreading depression is not associated with neuronal injury in the normal brain. *Brain research* 1988; **449**(1-2): 395-8.
25. von Bornstadt D, Houben T, Seidel JL, et al. Supply-demand mismatch transients in susceptible peri-infarct hot zones explain the origins of spreading injury depolarizations. *Neuron* 2015; **85**(5): 1117-31.
26. Hartings JA, Shuttleworth CW, Kirov SA, et al. The continuum of spreading depolarizations in acute cortical lesion development: Examining Leao's legacy. *Journal of cerebral blood flow and metabolism : official journal of the International Society of Cerebral Blood Flow and Metabolism* 2016.
27. Ayata C. Spreading depression and neurovascular coupling. *Stroke; a journal of cerebral circulation* 2013; **44**(6 Suppl 1): S87-9.
28. Hoffmann U, Ayata C. Neurovascular coupling during spreading depolarizations. *Acta neurochirurgica Supplement* 2013; **115**: 161-5.
29. Woitzik J, Hecht N, Pinczolits A, et al. Propagation of cortical spreading depolarization in the human cortex after malignant stroke. *Neurology* 2013; **80**(12): 1095-102.
30. Dreier JP. The role of spreading depression, spreading depolarization and spreading ischemia in neurological disease. *Nature medicine* 2011; **17**(4): 439-47.
31. Dreier JP, Korner K, Ebert N, et al. Nitric oxide scavenging by hemoglobin or nitric oxide synthase inhibition by N-nitro-L-arginine induces cortical spreading ischemia when K+ is increased in the subarachnoid space. *Journal of cerebral blood flow and metabolism : official journal of the International Society of Cerebral Blood Flow and Metabolism* 1998; **18**(9): 978-90.
32. Dreier JP, Ebert N, Priller J, et al. Products of hemolysis in the subarachnoid space inducing spreading ischemia in the cortex and focal necrosis in rats: a model for delayed ischemic neurological deficits after subarachnoid hemorrhage? *Journal of neurosurgery* 2000; **93**(4): 658-66.
33. Chesler M, Kaila K. Modulation of pH by neuronal activity. *Trends in neurosciences* 1992; **15**(10): 396-402.
34. Nedergaard M, Goldman SA, Desai S, Pulsinelli WA. Acid-induced death in neurons and glia. *The Journal of neuroscience : the official journal of the Society for Neuroscience* 1991; **11**(8): 2489-97.
35. Siesjo BK, Katsura KI, Kristian T, Li PA, Siesjo P. Molecular mechanisms of acidosis-mediated damage. *Acta neurochirurgica Supplement* 1996; **66**: 8-14.
36. Lipton P. Ischemic cell death in brain neurons. *Physiological reviews* 1999; **79**(4): 1431-568.
37. Selman WR, Lust WD, Pundik S, Zhou Y, Ratcheson RA. Compromised metabolic recovery following spontaneous spreading depression in the penumbra. *Brain research* 2004; **999**(2): 167-74.
38. Farkas E, Luiten PG. Cerebral microvascular pathology in aging and Alzheimer's disease. *Progress in neurobiology* 2001; **64**(6): 575-611.
39. Faber JE, Zhang H, Lassance-Soares RM, et al. Aging causes collateral rarefaction and increased severity of ischemic injury in multiple tissues. *Arteriosclerosis, thrombosis, and vascular biology* 2011; **31**(8): 1748-56.
40. Park L, Anrather J, Girouard H, Zhou P, Iadecola C. Nox2-derived reactive oxygen species mediate neurovascular dysregulation in the aging mouse brain. *Journal of cerebral blood flow and metabolism : official journal of the International Society of Cerebral Blood Flow and Metabolism* 2007; **27**(12): 1908-18.
41. Chen RL, Balami JS, Esiri MM, Chen LK, Buchan AM. Ischemic stroke in the elderly: an overview of evidence. *Nature reviews Neurology* 2010; **6**(5): 256-65.
42. Liu F, McCullough LD. Interactions between age, sex, and hormones in experimental ischemic stroke. *Neurochemistry international* 2012; **61**(8): 1255-65.

43. Ay H, Koroshetz WJ, Vangel M, et al. Conversion of ischemic brain tissue into infarction increases with age. *Stroke; a journal of cerebral circulation* 2005; **36**(12): 2632-6.
44. Popa-Wagner A, Badan I, Walker L, Groppa S, Patrana N, Kessler C. Accelerated infarct development, cytogenesis and apoptosis following transient cerebral ischemia in aged rats. *Acta neuropathologica* 2007; **113**(3): 277-93.
45. Farkas E, Bari F. Spreading depolarization in the ischemic brain: does aging have an impact? *The journals of gerontology Series A, Biological sciences and medical sciences* 2014; **69**(11): 1363-70.
46. Clark D, Institoris A, Kozak G, et al. Impact of aging on spreading depolarizations induced by focal brain ischemia in rats. *Neurobiology of aging* 2014; **35**(12): 2803-11.
47. LaManna JC, McCracken KA. The use of neutral red as an intracellular pH indicator in rat brain cortex in vivo. *Analytical biochemistry* 1984; **142**(1): 117-25.
48. Chen G, Gao W, Reinert KC, et al. Involvement of kv1 potassium channels in spreading acidification and depression in the cerebellar cortex. *Journal of neurophysiology* 2005; **94**(2): 1287-98.
49. Chen G, Hanson CL, Ebner TJ. Functional parasagittal compartments in the rat cerebellar cortex: an in vivo optical imaging study using neutral red. *Journal of neurophysiology* 1996; **76**(6): 4169-74.
50. Voipio J, Kaila K. Interstitial PCO2 and pH in rat hippocampal slices measured by means of a novel fast CO2/H(+)-sensitive microelectrode based on a PVC-gelled membrane. *Pflugers Archiv : European journal of physiology* 1993; **423**(3-4): 193-201.
51. Farkas E, Pratt R, Sengpiel F, Obrenovitch TP. Direct, live imaging of cortical spreading depression and anoxic depolarisation using a fluorescent, voltage-sensitive dye. *Journal of cerebral blood flow and metabolism : official journal of the International Society of Cerebral Blood Flow and Metabolism* 2008; **28**(2): 251-62.
52. Sun X, Wang Y, Chen S, Luo W, Li P, Luo Q. Simultaneous monitoring of intracellular pH changes and hemodynamic response during cortical spreading depression by fluorescence-corrected multimodal optical imaging. *NeuroImage* 2011; **57**(3): 873-84.
53. Obrenovitch TP, Chen S, Farkas E. Simultaneous, live imaging of cortical spreading depression and associated cerebral blood flow changes, by combining voltage-sensitive dye and laser speckle contrast methods. *NeuroImage* 2009; **45**(1): 68-74.
54. Domoki F, Zolei D, Olah O, et al. Evaluation of laser-speckle contrast image analysis techniques in the cortical microcirculation of piglets. *Microvascular research* 2012; **83**(3): 311-7.
55. Dreier JP, Petzold G, Tille K, et al. Ischaemia triggered by spreading neuronal activation is inhibited by vasodilators in rats. *The Journal of physiology* 2001; **531**(Pt 2): 515-26.
56. Ruusuvuori E, Kaila K. Carbonic anhydrases and brain pH in the control of neuronal excitability. *Sub-cellular biochemistry* 2014; **75**: 271-90.
57. Hertelendy P, Menyhart A, Makra P, et al. Advancing age and ischemia elevate the electric threshold to elicit spreading depolarization in the cerebral cortex of young adult rats. *Journal of cerebral blood flow and metabolism : official journal of the International Society of Cerebral Blood Flow and Metabolism* 2016.
58. Varga DP, Puskas T, Menyhart A, et al. Contribution of prostanoid signaling to the evolution of spreading depolarization and the associated cerebral blood flow response. *Scientific reports* 2016; **6**: 31402.
59. Duverger D, MacKenzie ET. The quantification of cerebral infarction following focal ischemia in the rat: influence of strain, arterial pressure, blood glucose concentration, and age. *Journal of cerebral blood flow and metabolism : official journal of the International Society of Cerebral Blood Flow and Metabolism* 1988; **8**(4): 449-61.
60. Fox G, Gallacher D, Shevde S, Loftus J, Swayne G. Anatomic variation of the middle cerebral artery in the Sprague-Dawley rat. *Stroke; a journal of cerebral circulation* 1993; **24**(12): 2087-92; discussion 92-3.
61. Rubino GJ, Young W. Ischemic cortical lesions after permanent occlusion of individual middle cerebral artery branches in rats. *Stroke; a journal of cerebral circulation* 1988; **19**(7): 870-7.

62. Bere Z, Obrenovitch TP, Bari F, Farkas E. Ischemia-induced depolarizations and associated hemodynamic responses in incomplete global forebrain ischemia in rats. *Neuroscience* 2014; **260**: 217-26.
63. Farkas E, Obrenovitch TP, Institoris A, Bari F. Effects of early aging and cerebral hypoperfusion on spreading depression in rats. *Neurobiology of aging* 2011; **32**(9): 1707-15.
64. Maslarova A, Alam M, Reiffurth C, Lapilover E, Gorji A, Dreier JP. Chronically epileptic human and rat neocortex display a similar resistance against spreading depolarization in vitro. *Stroke; a journal of cerebral circulation* 2011; **42**(10): 2917-22.
65. Bere Z, Obrenovitch TP, Kozak G, Bari F, Farkas E. Imaging reveals the focal area of spreading depolarizations and a variety of hemodynamic responses in a rat microembolic stroke model. *Journal of cerebral blood flow and metabolism : official journal of the International Society of Cerebral Blood Flow and Metabolism* 2014; **34**(10): 1695-705.
66. Hansen AJ, Zeuthen T. Extracellular ion concentrations during spreading depression and ischemia in the rat brain cortex. *Acta physiologica Scandinavica* 1981; **113**(4): 437-45.
67. Rossi DJ, Brady JD, Mohr C. Astrocyte metabolism and signaling during brain ischemia. *Nature neuroscience* 2007; **10**(11): 1377-86.
68. Windmuller O, Lindauer U, Foddis M, et al. Ion changes in spreading ischaemia induce rat middle cerebral artery constriction in the absence of NO. *Brain : a journal of neurology* 2005; **128**(Pt 9): 2042-51.
69. Warner DS, Sheng H, Batinic-Haberle I. Oxidants, antioxidants and the ischemic brain. *The Journal of experimental biology* 2004; **207**(Pt 18): 3221-31.
70. Mayhan WG, Arrick DM, Sharpe GM, Sun H. Age-related alterations in reactivity of cerebral arterioles: role of oxidative stress. *Microcirculation* 2008; **15**(3): 225-36.
71. Ungvari Z, Kaley G, de Cabo R, Sonntag WE, Csiszar A. Mechanisms of vascular aging: new perspectives. *The journals of gerontology Series A, Biological sciences and medical sciences* 2010; **65**(10): 1028-41.
72. Lapi D, Colantuoni A. Remodeling of Cerebral Microcirculation after Ischemia-Reperfusion. *Journal of vascular research* 2015; **52**(1): 22-31.
73. Chen G, Hanson CL, Ebner TJ. Optical responses evoked by cerebellar surface stimulation in vivo using neutral red. *Neuroscience* 1998; **84**(3): 645-68.
74. Chesler M, Kraig RP. Intracellular pH of astrocytes increases rapidly with cortical stimulation. *The American journal of physiology* 1987; **253**(4 Pt 2): R666-70.
75. Zhou N, Gordon GR, Feighan D, MacVicar BA. Transient swelling, acidification, and mitochondrial depolarization occurs in neurons but not astrocytes during spreading depression. *Cerebral cortex* 2010; **20**(11): 2614-24.
76. Walz W, Mukerji S. Lactate release from cultured astrocytes and neurons: a comparison. *Glia* 1988; **1**(6): 366-70.
77. Katsura K, Asplund B, Ekholm A, Siesjo BK. Extra- and Intracellular pH in the Brain During Ischaemia, Related to Tissue Lactate Content in Normo- and Hypercapnic rats. *The European journal of neuroscience* 1992; **4**(2): 166-76.
78. Kraig RP, Ferreira-Filho CR, Nicholson C. Alkaline and acid transients in cerebellar microenvironment. *Journal of neurophysiology* 1983; **49**(3): 831-50.
79. Obrenovitch TP, Garofalo O, Harris RJ, et al. Brain tissue concentrations of ATP, phosphocreatine, lactate, and tissue pH in relation to reduced cerebral blood flow following experimental acute middle cerebral artery occlusion. *Journal of cerebral blood flow and metabolism : official journal of the International Society of Cerebral Blood Flow and Metabolism* 1988; **8**(6): 866-74.
80. Rosenthal M, Somjen G. Spreading depression, sustained potential shifts, and metabolic activity of cerebral cortex of cats. *Journal of neurophysiology* 1973; **36**(4): 739-49.
81. Nowicki JP, Assumel-Lurdin C, Duverger D, MacKenzie ET. Temporal evolution of regional energy metabolism following focal cerebral ischemia in the rat. *Journal of cerebral blood flow and metabolism : official journal of the International Society of Cerebral Blood Flow and Metabolism* 1988; **8**(4): 462-73.

82. Menyhart A, Makra P, Szepes BE, et al. High incidence of adverse cerebral blood flow responses to spreading depolarization in the aged ischemic rat brain. *Neurobiology of aging* 2015; **36**(12): 3269-77.
83. Back T, Hoehn M, Mies G, et al. Penumbral tissue alkalosis in focal cerebral ischemia: relationship to energy metabolism, blood flow, and steady potential. *Annals of neurology* 2000; **47**(4): 485-92.
84. Peek KE, Lockwood AH, Izumiyama M, Yap EW, Labove J. Glucose metabolism and acidosis in the metabolic penumbra of rat brain. *Metabolic brain disease* 1989; **4**(4): 261-72.
85. Siqueira IR, Cimarosti H, Fochesatto C, Salbego C, Netto CA. Age-related susceptibility to oxygen and glucose deprivation damage in rat hippocampal slices. *Brain research* 2004; **1025**(1-2): 226-30.
86. Yemisci M, Gursoy-Ozdemir Y, Vural A, Can A, Topalkara K, Dalkara T. Pericyte contraction induced by oxidative-nitrative stress impairs capillary reflow despite successful opening of an occluded cerebral artery. *Nature medicine* 2009; **15**(9): 1031-7.
87. Hall CN, Reynell C, Gesslein B, et al. Capillary pericytes regulate cerebral blood flow in health and disease. *Nature* 2014; **508**(7494): 55-60.
88. Attwell D, Buchan AM, Charpak S, Lauritzen M, Macvicar BA, Newman EA. Glial and neuronal control of brain blood flow. *Nature* 2010; **468**(7321): 232-43.
89. Hopwood SE, Parkin MC, Bezzina EL, Boutelle MG, Strong AJ. Transient changes in cortical glucose and lactate levels associated with peri-infarct depolarisations, studied with rapid-sampling microdialysis. *Journal of cerebral blood flow and metabolism : official journal of the International Society of Cerebral Blood Flow and Metabolism* 2005; **25**(3): 391-401.
90. Tombaugh GC. Mild acidosis delays hypoxic spreading depression and improves neuronal recovery in hippocampal slices. *The Journal of neuroscience : the official journal of the Society for Neuroscience* 1994; **14**(9): 5635-43.